ORIGINAL ARTICLE

Joint estimation of sea ice and atmospheric state from microwave imagers in operational weather forecasting

Alan J. Geer[1*] |

This work has not yet been peer-reviewed and is provided for timely dissemination of scholarly and technical work on a noncommercial basis. Copyright and all rights therein are maintained by ECMWF. This work may not be reposted without explicit permission of the copyright owner.[1]

[1]ECMWF, Research Department, Reading, Berkshire, RG2 9AX, UK

Correspondence
Alan Geer, Research Department, ECMWF, Reading, Berkshire, RG2 9AX, UK
Email: alan.geer@ecmwf.int

Funding information

Satellite-observed microwave radiances provide information on both surface and atmosphere. For operational weather forecasting, information on atmospheric temperature, humidity, cloud and precipitation is directly inferred using all-sky radiance data assimilation. In contrast, information on the surface state, such as sea surface temperature (SST) and sea ice fraction, is typically provided through third-party retrieval products. Scientifically, this is a sub-optimal use of the observations, and practically it has disadvantages such as time delays of more than 48 hours. A better solution is to jointly estimate the surface and atmospheric state from the radiance observations. This has not been possible until now due to incomplete knowledge of the surface state and the radiative transfer that links this to the observed radiances. A new approach based on an empirical state and empirical sea ice surface emissivity model is used here to add sea ice

[*] Sole author.

state estimation, including sea ice concentration (SIC), to the European Centre for Medium-range Weather Forecasts atmospheric data assimilation system. The sea ice state is estimated using augmented control variables at the observation locations. The resulting SIC estimates are of good quality and they highlight apparent defects in the existing OCEAN5 sea ice analysis. The SIC estimates can also be used to track giant icebergs, which may provide a novel maritime application for passive microwave radiances. Further, the SIC estimates should be suitable for onward use in coupled ocean-atmosphere data assimilation. There is also increased coverage of microwave observations in the proximity of sea ice, leading to improved atmospheric forecasts out to day 4 in the Southern Ocean.

KEYWORDS
sea ice, giant iceberg, microwave radiance, empirical state, surface emissivity

1 | INTRODUCTION

Observations of the earth system from ground-based platforms and satellite radiances provide the initial state and boundary conditions for earth system forecasting. Typically the observations are combined with model forecasts using a data assimilation system. The most extensive use of observations is in atmospheric data assimilation, where satellite radiances provide the majority of the information globally (Bormann et al., 2017). These radiances can be assimilated in all-sky conditions (clear, cloudy and precipitating situations) to improve atmospheric winds, temperature, humidities and hydrometeors (Geer et al., 2017, 2018). But satellite radiances also provide information on many other parts of the earth system, particularly on surface variables like soil moisture, vegetation, snow cover, skin temperature and sea ice concentration (SIC), which is a target of the current work. Information on surface variables is typically obtained through third-party retrievals and analyses, outside the main atmospheric data assimilation process at forecasting centres. However, this incurs significant practical and scientific problems.

From the practical point of view, the existing operational processing chains are long and complex and can generate delays of at least 48 hours compared to the validity time of the observations (e.g. Baordo and Geer, 2015; Browne et al., 2019; Geer, 2023). The complexity of these processing chains has also resulted in poor robustness at times. By contrast, the observation processing for atmospheric data assimilation at weather centres is highly robust, with a huge diversity of observational sources, multiple layers of quality control, and attention paid to ensuring the most timely use of observations (e.g. Lean et al., 2021). If the processing of surface-related observations could be brought into this framework it would have great practical benefits.

From the scientific side, the fundamental problem with using surface retrievals external to the data assimilation system is that observations which are sensitive to the surface are usually sensitive to the atmosphere too. This can lead to the situation where the same satellite observation is used directly in the atmospheric analysis and indirectly in the

surface state retrievals, which is sub-optimal. For example the surface state retrieval could be based on an out-of-date estimate of the atmospheric state, or a climatology (e.g. Meissner et al., 2023). Similar problems with the assimilation of satellite temperature retrievals drove the development of direct radiance assimilation at weather centres (Eyre et al., 2020) with well known benefits to the quality of weather forecasts (Bauer et al., 2015). There are theoretical ways to make an optimal analysis using retrievals (e.g. Migliorini et al., 2008) but they rely on an optimal estimation framework throughout the processing chain and they bring a heavy burden of additional matrices to be passed around with the retrievals. A cleaner way to make optimal use of the observations is to jointly estimate the atmospheric and surface state from the radiances. This is one of the main motivations for developing coupled data assimilation (DA) across different earth system components (e.g. de Rosnay et al., 2022; McNally et al., 2022). However, coupled DA has its own complexity issues and is still in development. So the current work takes the simpler but still potentially optimal approach to extend an atmospheric data assimilation system to infer the state of the surface as well, in particular the state of the sea ice.

Atmospheric data assimilation systems typically do not directly include (or couple to) prognostic surface models. Sea ice analyses are typically made separately from the atmosphere (e.g. Buehner et al., 2016; Mu et al., 2020) and this includes the current sea ice analysis at the European Centre for Medium-range Weather Forecasts (ECMWF) (Zuo et al., 2019). One of the great benefits of four-dimensional (4D) assimilation is the constraint of the forecast model, but in an uncoupled atmospheric DA, this only applies to the atmosphere and the relevant surface fields are held constant. An alternative is to add the required additional fields to the control vector in observation space at observation locations: an augmented control vector approach. This allows the analysis to fit the surface state at the exact moment and in the exact field of view of the observation. Such a technique has been used for several decades at ECMWF in the skin temperature 'sink variable' for clear-sky radiance assimilation and was also used as a way to estimate cloud variables for assimilating overcast infrared radiances (McNally, 2009). A two-dimensional auxiliary control variable has been tested to allow a skin temperature analysis within an atmospheric data assimilation system (Massart et al., 2021) but for the current work an observation-space approach is used. The intention is then to pass the sea ice retrieval to the ocean and sea ice analysis, to replace the external sea ice retrievals that are currently used. Improved sea ice analyses should be useful in their own right as well as to improve the quality of ocean and atmosphere forecasts (the influence of sea ice on weather and climate is explored in e.g. Chripko et al., 2021). An equivalent approach is already in development to make use of skin temperature retrievals at observation locations (McNally et al., 2022). This initial work on sea ice implements the process as far as retrieving sea ice in the auxilliary control variable.

Further motivation for improving the use of surface information in atmospheric data assimilation is to extend the use of satellite radiances. Observations with strong surface sensitivity have typically been used over the open ocean but not over sea ice or land surfaces. Due to the need to screen out the more strongly surface-sensitive satellite data over these surfaces, and due to increased errors in the data that is retained, the satellite contribution to northern hemisphere forecast quality is much reduced in the winter (e.g. Lawrence et al., 2019). Recent work has extended the coverage of satellite data over coastlines, high latitudes and land surfaces, using the existing frameworks for satellite data assimilation, with clear benefit to forecast quality (e.g. Lonitz et al., 2022; Geer et al., 2022). However, sea ice, snow, desert and high altitude surfaces remain too difficult to use with channels that are strongly sensitive to the surface. The efforts to improve this situation are known as 'all-sky all-surface assimilation'.

The motivation to use more surface information directly through radiance assimilation is clear, but there are heavy scientific challenges in doing so, particularly the need to link the surface state to the observed radiance through a radiative transfer model. The first big problem is that many of the state variables that affect the radiative transfer are not well known: in the case of sea ice, the temperature and moisture profile of the sea-ice and its snow cover, and the microphysical properties of these layers, such as grain structure, all strongly affect the surface emission. Second,

even if these variables were perfectly known, there is also a relative lack of accuracy of current models for radiative transfer in the surface media (e.g. in sea-ice, soil, snow and vegetation). Typically snow radiative transfer modelling, based on physical snow model inputs, has been limited in accuracy above 20 GHz (e.g. Hirahara et al., 2020). Recent developments have shown accuracy to around 200 GHz under some conditions (Sandells et al., 2023), but this is based on detailed snow profiles from a research site, so it could be difficult to replicate more globally. The situation can be seen as a chicken and egg problem: better global analyses of surface properties could help develop improved surface radiative transfer models, but those global analyses require satellite observations and hence require surface radiative transfer models to be able to make the required satellite retrievals or analyses.

A solution to the chicken and egg problem has been found in the combination of machine learning and data assimilation to simultaneously learn from the observations both the unknown physical state of the surface and the forward model for the radiative transfer (Geer, 2023). The compromise is that both the physical state and the forward model are empirical. The current work takes a trained empirical sea ice surface emissivity model from that work in order to allow surface-sensitive microwave observations to be assimilated over and in proximity to sea ice in the atmospheric four-dimensional variational data assimilation (4D-Var) at ECMWF. As mentioned above, this can be done using observation-space auxiliary control variables to estimate both the SIC and some additional empirical variables that describe the physical state of the sea ice. This is done at the locations of Advanced Microwave Scanning Radiometer 2 (AMSR2) and the GPM Microwave Imager (GMI) observations. This article describes the sea ice sink variable framework within the ECMWF atmospheric data assimilation system (methodology in Sec. 2) along with results including improved observational coverage (Sec. 3.1), better simulations of observations (Sec. 3.2), a good quality sea ice analysis as compared to existing analyses and in giant iceberg case studies (Sec. 3.3) and improved atmospheric forecasts (Sec. 3.4). Section 4 concludes.

2 | METHOD

2.1 | New sea ice assimilation framework

Geer (2023) simultaneously estimated daily maps of the sea ice state and a new empirical model for the sea ice surface emissivity, based on a year of AMSR2 observations between August 2020 and July 2021 and ECMWF atmospheric and surface fields, using a combination of machine learning and data assimilation. The output from that work to the current one is the mixed surface emissivity model illustrated in Fig. 1 as adapted for the assimilation of AMSR2 and GMI observations in the 4D-Var atmospheric data assimilation framework (ECMWF, 2023, more details in Sec. 2.3). The physical part of the model computes the channel-dependent (vector) mixed surface emissivity $\mathbf{e}$, which depends on the sea ice concentration C_{ice} as well as the surface emissivities of ocean water $\mathbf{e}_{\text{water}}$ and sea ice surfaces $\mathbf{e}_{\text{ice}}$,

$$\mathbf{e} = (1 - C_{\text{ice}})\mathbf{e}_{\text{water}} + C_{\text{ice}}\mathbf{e}_{\text{ice}}. \tag{1}$$

The ocean water emissivity is modelled using the physical model SURFEM-ocean (Kilic et al., 2023), driven by forecast model fields such as skin temperature and 10m wind speed. These come from the ECMWF atmospheric forecast model within the Integrated Forecasting System (IFS). The sea ice surface emissivity is simulated using the empirical part of the model, to be described shortly. The natural contrast in surface emissivity between ocean water (typically low emissivity) and surfaces covered in snow or ice (typically higher emissivity, at least at mid microwave frequencies) is what allows the sea ice concentration to be determined from Eq. 1. However, the physics of this situation means that what is defined as sea ice concentration in this work includes iceberg ice and excludes any melt ponds, which will

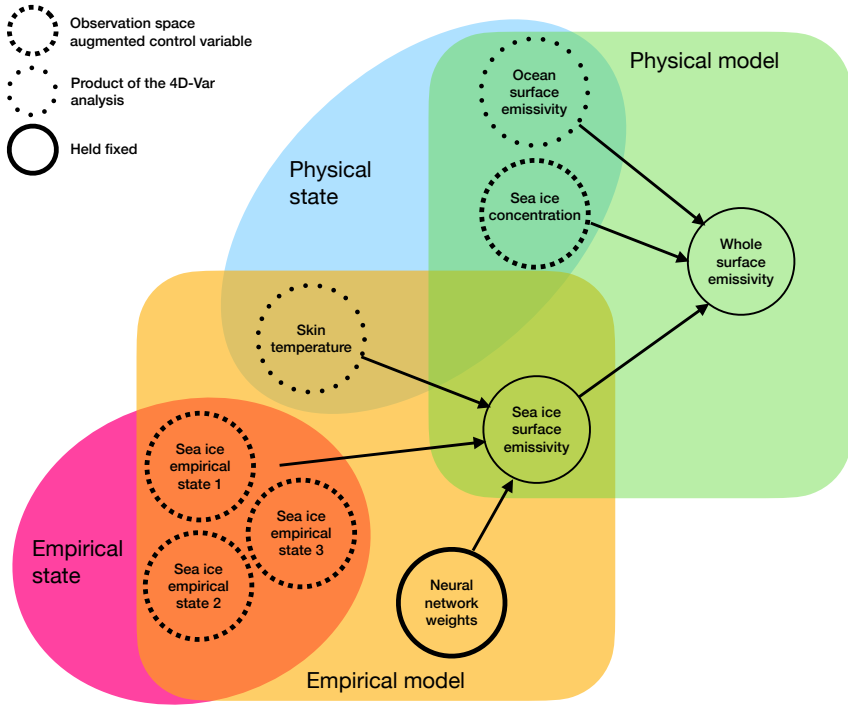

FIGURE 1 The empirical-physical model for mixed surface emissivity in the field of view of view of one microwave imager observation. Circles indicate variables: these are scalars except the neural network weights, of which there are 50, and the surface emissivity variables, which represent 10 frequencies and polarisations measured by microwave imagers between 10 GHz and 89 GHz.

be observed as open ocean.

The empirical part of the new model is used to determine the frequency or channel-dependent surface emissivity of the sea ice, which is highly variable depending on the surface conditions. This component is a linear single layer dense neural network (equivalently, a linear regression model) which takes three empirical inputs representing the physical and microphysical properties of the sea ice relevant to the surface emissivity as well as the skin temperature from the IFS model. The empirical input parameters do not have an exact physical meaning but as shown in Geer (2023) they vary with known physical characteristics of the sea ice, such as the differences between new and multi-year ice.

In potential sea ice areas, the mixed surface emissivity from this model, along with the skin temperature, are the surface boundary conditions for the RTTOV atmospheric radiative transfer model (Radiative Transfer for TOVS; Saunders et al., 2018). RTTOV simulates the effects of atmospheric gas absorption (primarily water vapour) and the scattering and absorption from clouds and precipitation, based on the atmospheric profile from the IFS model at the observation location. The output of RTTOV is the top of atmosphere brightness temperatures observed by the relevant satellite instrument. RTTOV also provides gradient models, as does the new sea ice component, to allow 4D-Var to adjust the analysed surface and atmospheric state to bring the simulated observations closer to the real observations from GMI and AMSR2, along with fitting all other atmospheric observations that are being assimilated

(see Sec. 2.3). The variables with dashed outlines are adjusted within the data assimilation, with square dashes indicating variables that are estimated independently at each observation location (observation space augmented control variables) and round dots indicating variables that are updated indirectly by 4D-Var adjusting the atmospheric forecast trajectory. This latter is done indirectly by adjusting the initial atmospheric conditions for the forecast trajectory, namely the surface pressure and the 3D fields of temperature, humidity, horizontal wind and ozone, which are the main control variables of 4D-Var. The 50 neural network weights that comprise the linear offline-trained empirical sea ice surface emissivity model are held fixed. One of the biggest problems of using microwave radiances over sea ice has been the unknown sea ice surface emissivity; this is now provided by the empirical model, but it is necessary for 4D-Var to simultaneously estimate the empirical sea ice state variables which describe the radiatively-relevant physical and microphysical characteristics of the sea ice.

The sea ice assimilation framework, with four observation-space augmented control variables and the empirical-physical model of Fig. 1, is activated for selected channels of GMI and AMSR2 over ocean surfaces if the background sea surface temperature is lower than 277.0 K. Any scene with a land fraction greater than 0.01 is excluded and treated in the existing framework for all-sky microwave assimilation over land (Geer et al., 2022). All-sky assimilation over 'open' ocean surfaces is done the same way as before, with the ocean surface emissivity provided solely by SURFEM-ocean and without any observation space augmented control variables. Sea ice assimilation is only applied to AMSR2 and GMI and other microwave imagers currently available in the ECMWF system are excluded: SSMIS (Special Sensor Microwave Imager Sounder Kunkee et al., 2008) because it does not have the 10 GHz channel that is used to estimate the background sea ice concentration; MWRI (Micro-Wave Radiation Imager) because it has been excluded from assimilation since May 2022 due to orbit-dependent biases (Scanlon et al., 2023). The results presented in this work are mainly from AMSR2, given its full polar coverage, but the impact on GMI utilisation is also important.

2.2 | Observation-space augmented control variables

The background value for the sea ice concentration control variable is taken from a sea ice concentration retrieval rather than the available sea ice estimate from the ECMWF ocean analysis, OCEAN5 (Zuo et al., 2019). The OCEAN5 estimate is a forecast valid at the correct time but is in practice around 48 h - 72 h behind instantaneous observations (Geer, 2023) due to delays in the arrival of its input sea ice analyses, as well as a possible slowness of the underlying sea ice model to adapt to changed conditions. This means it has such large sea ice position errors in some places that many observations would be rejected because of the resulting large background departures (up to around ±100K). Hence OCEAN5 does not provide a viable background sea ice concentration for assimilating microwave radiances. The alternative is a retrieval based on inverting Eq. 1 for the 10v channel only. The mixed surface emissivity is also retrieved dynamically from the observations as part of the previous way of using observations over sea ice (Baordo and Geer, 2016), giving $e_{ret,10v}$. It is assumed the sea ice emissivity in channel 10v, $e_{ice,10v}$, is a constant 0.93 (Lee et al., 2017). As in Eq. 1 the SURFEM-ocean model (Kilic et al., 2023) provides the ocean water surface emissivity, here $e_{water,10v}$ for the 10v channel. Hence:

$$C_{ice} = \frac{e_{ret,10v} - e_{water,10v}}{e_{ice,10v} - e_{water,10v}} \tag{2}$$

If the denominator is negative, C_{ice} is set to zero, and if it is outside physical bounds, it is reset to the nearest bound (0 or 1).

The background values for the three empirical variables describing the state of the sea ice are set to zero. Background error standard deviations are set to 0.25 for the sea ice concentration and 0.34, 0.34 and 0.3 for the empirical

state variables. The latter is based on the covariance matrix of the empirical state variables after training of the offline physical-empirical network (Geer, 2023) but with two modifications: it ignores correlations between the variables, and it doubles the error standard deviations. These choices were determined by trial and error during a rapid prototyping phase, in conjunction with tuning the observation errors (see Secs. 2.3 and 2.3.1). The chosen configuration appeared to help the sea ice emissivity model better fit the observations in the context of 4D-Var. However, no systematic investigation of the optimum error settings has been performed.

Because the augmented control variable in 4D-Var can only use a Gaussian background error model, it is not possible to suppress unphysical values of SIC in the way it was done by Geer (2023). Instead, any values of SIC that evolve to a value outside the bounds 0 and 1 are reset to the nearest value within bounds, during the trajectory update (outer loop) phase of 4D-Var.

The use of observation-space control variables is an important difference from the empirical-physical training process used by Geer (2023), which only estimated daily values for the four state variables, and therefore suppressed any sub-daily variability in the surface properties. By contrast, the implementation in 4D-Var gives greater scope to fit the observations. This gives a good opportunity to explore the sub-daily variability in the sea ice state (Sec. 3.3.3) which was not explored in the previous work.

2.3 | Testing framework

The sea ice developments in this work are intended for operational implementation within cycle 49r1 of the IFS in mid 2024. The developments are tested within the atmospheric data assimilation system on top of a baseline (or Control) that represents the previous operational cycle (48r1; ECMWF, 2023) plus most of the upgrades intended for 49r1 in the area of satellite microwave data assimilation. This baseline IFS configuration uses an atmospheric resolution of TCo399 (about 25 km horizontally) which is reduced compared to the operational resolution TCo1279 (about 9 km). The atmospheric data assimilation system is a non-overlapping 12-hour window 4D-Var with three inner loops up to TL255 resolution (40 km) which omits the additional complexities of continuous data assimilation in the operational system (Lean et al., 2021). The 12 h analysis windows run from 0900 to 2100 UTC and from 2100 to 0900 UTC, with the main 4D-Var control variables being the atmospheric state at the beginning of these windows. Deterministic 10-day forecasts are launched twice a day from these windows with the start times of 0000 and 1200 UTC.

The background errors for data assimilation are derived from the operational ensemble of data assimilations (Bonavita et al., 2016) and are thus the same in both control and experiment. The sea surface temperature (SST) and sea ice concentration (SIC) initial conditions are derived from the preceding analysis of the OCEAN5 operational assimilation system (Zuo et al., 2019) which assimilates the OSTIA daily sea ice analysis (Operational Sea Surface Temperature and Sea Ice Analysis; Good et al., 2020) into an ocean model including the LIM2 sea ice model (Louvain-la-Neuve sea ice model; Timmermann et al., 2005). Within the data assimilation window, the sea ice concentration is not evolved and remains constant, but the skin temperature over sea ice (and land) is adjusted within the atmospheric forecast model according to energy balance and other physical considerations (ECMWF, 2023, the skin temperature over open ocean is not adjusted by 4D-Var and instead comes from the OSTIA SST analysis, at least at the high latitudes relevant to this work). Over sea ice especially there are known issues with the skin temperature (Zampieri et al., 2023) but the new sea ice surface emissivity model is intended to work with, and is trained on, these skin temperatures. It should also be noted that the OCEAN5 sea ice boundary conditions for the model are the same in both the control and the experiment, and OCEAN5 itself is driven by the operational atmospheric forecast. This means that the current experiments are not weakly coupled (Browne et al., 2019) and do not test the feedback of the new sea ice observations into the ocean component, which will be the subject of further work.

The atmospheric data assimilation system assimilates a full global observing system comprising ground-based measurements such as aircraft, radiosondes and surface stations, and satellite observations, which comprise infrared and microwave radiances, scatterometers, radio occultation bending angles, atmospheric motion vectors and line of sight Doppler wind measurements. Concially scanning microwave imagers, the focus of this work, form a subset of the microwave observations that are mainly intended for sensing surface properties and atmospheric humidity, cloud and precipitation. However, as discussed in the introduction, the strongly-surface sensitive channels are only used over oceans without sea-ice, and land areas excluding snow, high altitudes and dry soils (Lonitz et al., 2022; Geer et al., 2022). The only surface information that is currently inferred is the near-surface windspeed over ocean, which is obtained through the surface emissivity model SURFEM-ocean (Kilic et al., 2023; Geer et al., 2023). The aim of the current work is to extend the use of these observations for their atmospheric information content over and near sea-ice areas, and to better exploit their sea ice information content.

Compared to the previously documented IFS cycle 48r1 (ECMWF, 2023) and in particular superseding the latest fully documented configuration of the microwave assimilation (Geer et al., 2022) the IFS baseline includes two important changes. First, the RTTOV radiative transfer model is upgraded to version 13.2. This is mostly a non-scientific upgrade, except that the newly-available ocean surface emissivity component, SURFEM-ocean (Kilic et al., 2023) is activated in the IFS (Geer et al., 2023) in preference to FASTEM-6 (Kazumori and English, 2015). Second is to move from an 80 km resolution superobservation strategy for the microwave imagers to 40 km, which was particularly intended to provide a better resolution in the new surface analysis. A number of other new extensions to the use of SSMIS, AMSU-A and microwave humidity sounders (Scanlon et al., 2023; Duncan et al., 2022, 2023) are included in the baseline system but these are less directly relevant, since they do not fill the observational gaps at low levels over the sea ice and surrounding ocean, which are the target of the current work.

The control and sea ice configurations of the atmospheric data assimilation and forecasting system were compared for 12 months between 1st November 2021 and 31st October 2022. This was generated using two approximately 6-month long experiments in each configuration: one starting from 20th October 2021 and running until the end of April 2022 and another starting 19th April and running until the end of October 2022. The experiments were in each case initialised from the ECMWF operational forecast, with the initial 12 days discarded for spinup. Additionally, just in Sec. 3.3.4, results are shown from an equivalent set of experiments during autumn 2020. The main 12 month period is chosen to avoid the training period for the empirical sea ice surface emissivity model (August 2020 to July 2021) in order to check that the new sea ice emissivity model can work outside its training period.

Note that, as already mentioned, the new configuration being tested here was developed during a rapid prototyping phase that was time-limited by the deadline for integration in the 49r1 operational cycle. Due to the cost of experimentation using 4D-Var, it is not possible to justify every implementation choice individually using further experimentation. The success of the combination of all these settings together should give reasonable confidence in this initial implementation, though it is likely that the settings and techniques could be improved further.

2.3.1 | Assimilation settings

Table 1 summarises the assimilation settings for AMSR2 and GMI over ocean in the new framework. These settings now vary depending on whether the scene is considered open ocean or whether the new sea ice approach is active, which depends on the 277.0 K SST threshold. Over open ocean, the standard cloud-dependant observation error models are applied (Kazumori, 2016; Lean et al., 2017, AMSR2 and GMI respectively). In the sea ice framework, the detailed form of the observation error is still not known, since as shown later, there are large error variations dependent on cloud, ocean surface conditions and the sea ice state. Hence the observation errors, shown in Table 2,

TABLE 1 Assimilation settings for the ocean data assimilation pathways

	Open ocean	Possible sea ice
Selection	SST at background $\geq$ 277.0K	SST at background $<$ 277.0K
Observation errors	Cloud-dependent	Fixed: Table 2
Cold air outbreak screening	Yes	No
Sea ice screening	Yes	No
Background quality control	2.5 times observation error std. dev.	As ocean except the 10 GHz v-polarised channel (10v) uses 4.0 times std. dev.
Variational quality control	Yes	Yes
Thinning	1 in 8 superobs assimilated for atmosphere	1 in 8 superobs assimilated for atmosphere and surface
		Other 7 of 8 superobs assimilated for surface only

SST = sea surface temperature

are fixed and have been set partly by trial and error. These errors were inspired by the values used in the offline study (Geer, 2023) but they are 4 times larger in all channels except 10v. For this channel, the errors were inflated by a smaller multiple, reflecting the importance of this channel in constraining the SIC, and noting that the 10v channel is less vulnerable to the cold air outbreak errors described below. The observation errors are necessarily larger than in the offline study, both to deal with the cold air outbreak problem and to avoid damaging the atmospheric analysis in areas where the sea ice emissivity modelling has residual errors.

Over open ocean, there are two specific screening packages applied (Table 1). The first is because the IFS moist physics performs poorly in cold air outbreak regions (CAO; e.g. Forbes et al., 2016). The affected areas have background departure biases of around 10 K so they have had to be screened out. Sometimes there is no way for the assimilation system to fit these observations without making large temperature increments, to the extent that it can sometimes cause a forecast model explosion. The CAO rejection is based on low total column water vapour (< 8 kg m^{-2}) or low values of a lower tropospheric stability parameter (Lonitz and Geer, 2015). In the new sea ice framework, CAOs had to be included because otherwise a lot of data would be rejected from the sea ice pathway. As previously mentionedm this is one reason the observation errors are in general much larger than over open ocean. Further, the ability to adjust the surface emissivity using the sea ice model acts a 'safety valve' that can absorb the CAO biases where they occur, so they are less dangerous to assimilate. As will be explained later, this means that the missing CAO cloud can be fitted by generating spurious low-concentration sea ice. Although this is scientifically imperfect, it is an important practical change that significantly boosts the atmospheric forecast impact of the sea ice assimilation (Sec. 3.4).

The pre-existing sea-ice screening package (Geer et al., 2022) is retained for open ocean areas, just in case sea ice is present at SSTs above 277.0 K. Other more general quality control aspects are retained in both open ocean and sea ice. These are the background quality control, which rejects data with background departures greater than a multiple of the observation error, ordinarily 2.5 times, and variational quality control (Andersson and Järvinen, 1998). The only change for sea ice is that the background quality control for the 10v channel is relaxed from 2.5 times to 4.0 times to

TABLE 2 Channel usage over oceans in the sea ice assimilation configuration

Channel	AMSR2 ocean	AMSR2 sea ice	GMI ocean	GMI sea ice	Sea ice observation error [K]
10v	x	S	x	S	7.0
10h	x	S	x	S	20.0
19v	A	S	A	S	11.0
19h	A	S	A	S	21.0
24v	A	S	A	S	12.0
24h	A	S	-	-	20.0
37v	A	S	A	S	22.0
37h	x	x	x	x	x
89v	A	S	A	S	23.0
89h	x	x	x	x	x
166v	-	-	A	x	x
166h	-	-	A	x	x
183±7v	-	-	A	x	x
183±3v	-	-	A	A	Variable

x, unused or passive in the data assimilation; A, active for atmospheric data assimilation; S, active for sea ice and atmospheric data assimilation; -, channel does not exist.
AMSR2 channels 6v, 6h, 7v, 7h are not included as they are not currently used in 4D-Var.
Channel codes like '10v' include an approximate frequency in GHz along with the polarisation, either 'v' for vertical or 'h' for horizontal.

retain observations with larger discrepancies between background and observed sea ice.

Table 2 shows the channel usage for AMSR2 and GMI in the new sea ice framework. The usage depends on whether the scene is open ocean or sea ice according to the SST threshold. The new sea ice approach is applied to the channels for which the empirical sea ice surface emissivity model is valid, namely channels between 10v and 89h. The 10 GHz channels 10v and 10h are activated for the first time in the IFS to support the new framework, but they are not activated over open ocean areas. Following existing treatment over ocean, horizontally polarised channels at 37 GHz and 89 GHz (37h and 89h) are not activated in sea ice areas, due to the very strong sensitivity to cloud liquid water. The 166 GHz and 183 GHz channels of GMI are actively assimilated, in the same way as in the control, and they are not covered by the new framework. In these channels, the 277.0 K threshold for the sea ice is not relevant, but rather the pre-existing utilisation of observations is retained, as described in Geer et al. (2022). This means that the 183±3 GHz channel of GMI is active over sea ice but it uses the existing dynamic emissivity retrieval approach (Geer et al., 2014; Baordo and Geer, 2016), and it does not contribute to (or benefit from) the new sea ice approach. The 6 and 7 GHz channels of AMSR2 could contribute useful sea ice information in future but they are not yet included because the 40 km superobbing strategy is not appropriate to their relatively large fields of view.

Due to relatively large mean changes in the atmospheric analysis observed in early trials, particularly in the Weddel sea in Antarctic summer, an additional treatment for 'summer scattering' surfaces was added. In these situations, the sea ice emissivity model was failing to fit the observations, primarily in the 89 GHz channels. The 89v channel

was showing analysis departures of around +20 K during the day and -20 K during the night. During the night in these situations the real observations exhibited deep brightness temperature depressions, down to 200 K at 89v, with model-estimated skin temperatures around 270 - 272 K, suggesting a frozen surface (or at least a crust) that was generating strong scattering. During the day the observations were up to around 260 K at 89v, with skin temperatures of around 274 - 275 K, suggesting a strongly absorbing and wet surface snowpack. It is speculated that the offline-trained empirical model (Geer, 2023) was not able to capture this behaviour because it was restricted to estimating daily mean empirical surface properties and surface emissivity, and because the problematic areas seem to occur most clearly where the diurnal cycle is strong.

To partly deal with this 'freeze-thaw' issue in 4D-Var, the observation error was inflated beyond the Table 2 values in areas with skin temperatures greater than 269.0 K and with positive scattering indexes based on the difference in observed brightness temperatures between 19v and 89v channels, $T_{19v} - T_{89v}$. Note that this scattering index targets the re-frozen, strongly scattering surfaces rather than the thawed surfaces, since due to the observed sign of the mean changes in the analysis, it was the re-frozen surfaces that appeared to cause the main problem. The inflation was applied as a multiplicative scaling as a function of the scattering index, namely:

$$\sigma_{final} = \sigma_{ice}\left(1 + \frac{T_{19v} - T_{89v}}{30.0}\right); (T_{19v} - T_{89v}) > 0 \tag{3}$$

where σ_{final} was the final observation error standard deviation in any channel and σ_{ice} being the sea ice observation error from Table 2. When the scattering index is zero or negative, there is no change to the observation error. The scaling factor of 30.0 K in the denominator means that the observation error is doubled when the scattering index reaches 30.0 K. By downweighting the observations in these difficult summer situations with strong diurnal cycles, the rapid prototyping phase showed this was effective at removing the most obvious mean changes in the atmospheric analysis, though some issues remain (Sec. 3.2).

Variational bias correction (VarBC Dee, 2005) is used to remove systematic biases between the model and the observations, using a multiple linear bias model that is a function of various predictors. The usual set of bias predictors for surface-sensitive microwave imager channels is: a constant; skin temperature; total column water vapour; 4-order polynomial in scan position; surface wind speed. These predictors are by default global and estimated separately for each channel. The sea ice addition required the surface wind speed predictor to be changed so that it is effective only over open ocean, and not over sea ice or land. This had extremely minor side-effects for the bias correction of already-used AMSR2 and GMI data over land surfaces, but due to the very small size and location of these changes, it is clear they do not affect the main results of the study. Also, for AMSR2 only, the SIC is added as a further predictor, allowing a separation in the bias correction between open ocean and sea ice, to deal with known scene-temperature dependent biases that are seen for AMSR2 but not GMI (Geer et al., 2022; Berg et al., 2016). Channels 37v and 89v are assimilated over land surfaces too (Geer et al., 2022) and these channels have additional predictors for land-surface mask and skin temperature times land-surface mask (Geer et al., 2022).

In terms of thinning, it is not possible to assimilate every 40 km resolution superob for the atmosphere, due to suspected observation error correlations (Bormann et al., 2011). For atmospheric purposes, and following the standard approach over other surfaces, the observations are thinned to leave 1 in every 8 superobs for assimilation, using a pattern that leaves a roughly 100 km spacing between the observations that are active for atmospheric data assimilation. However, the surface analysis would benefit from the full 40 km resolution of the superobs, so in the sea ice pathway, all observations are active in data assimilation for the observation-space control variables, but only 1 in 8 observations are active for the atmosphere. This is achieved by artificially zeroing the gradients of the 4D-Var cost function with respect to atmospheric variables for the other 7 in 8 sea ice observations; these are referred to

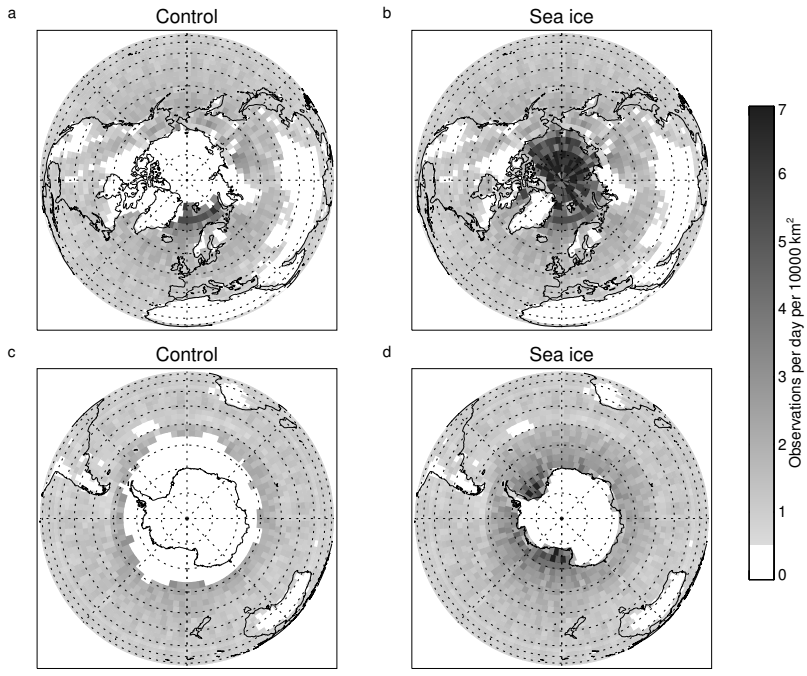

FIGURE 2 Number of observations per day per 10,000 km^2 during the period 1st - 5th June 2022, from AMSR2 channel 37v, in the control configuration (a,c) and the sea ice experiment (b,d). This shows the observations that are active for the atmosphere and not the 'surface only' observations. Dashed lines are every 10 degrees latitude and every 45 degrees longitude.

as 'surface only' observations: they benefit from the improvements to the atmospheric state during data assimilation, but they do not directly influence them.

3 | RESULTS

3.1 | Data utilisation

Figure 2 shows the benefit of the new sea ice pathway in terms of the number of observations available for atmospheric data assimilation in the AMSR2 37v channel. The selected period is in June, so the additional coverage in the Arctic is limited to a relatively small area. However, in the Antarctic, the control has few observations poleward of 60 degrees and the activation of sea ice observations fills this gap up to the edge of the Antarctic landmass. One noteworthy aspect of the figure is the way the coverage in polar regions is as much as 6 times higher than in the tropics and midlatitudes, due to the polar sun-synchronous orbit of the GCOM-W satellite. This illustrates the particular value in using polar-orbiting satellite observations in polar regions, and their potential to fill the winter data gap observed by Lawrence et al. (2019), once it is possible to use surface-sensitive radiances over sea ice and snow surfaces.

Figure 3 examines the impact on GMI numbers. GMI is in an inclined orbit which does not travel over the poles, but only reaches as high as approximately 70° latitude. This means it can also benefit significantly from activation over sea ice and possible sea ice areas, particularly in the southern hemisphere. Indeed, the addition of sea ice assimilation

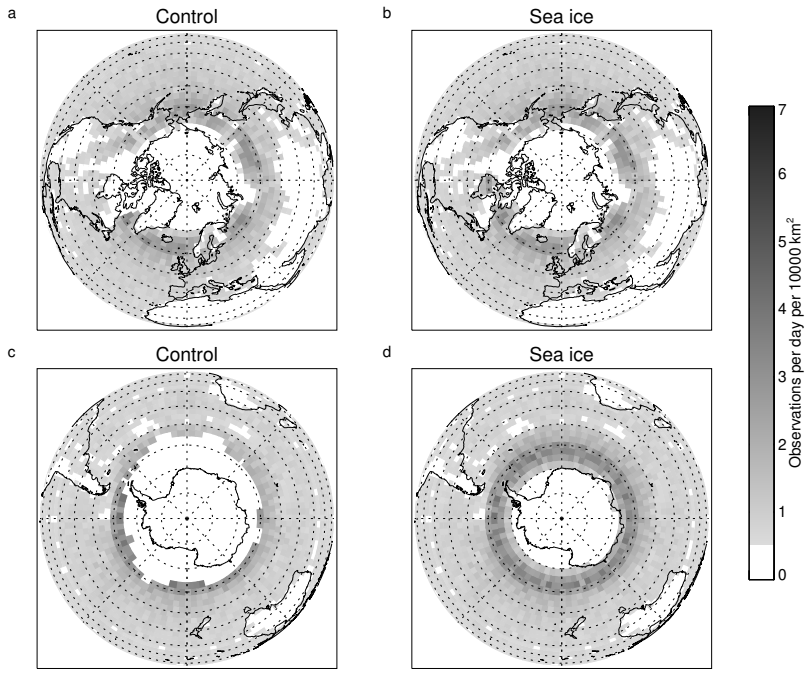

FIGURE 3 As Fig. 2 but from GMI channel 37v.

fills in the zone between approximately 60°S and 70°S with around 3 – 4 observations per day per 10,000 km^2.

Figure 4 shows the context of the sea ice pathway within the wider use of microwave imager data, based on all available superobs including those that are rejected for data assimilation, and looking at AMSR2 channel 19v. This figure is based on 12 h of data so the gaps between the satellite swaths are visible at lower latitudes, and at higher latitudes multiple orbits overlap. Background departures over sea ice in the control run are shown in panel a. The departure d is defined as the difference between observations T_{obs} and model simulations T_{sim} including the VarBC bias correction b:

$$d = T_{obs} - b - T_{sim} \tag{4}$$

These departures, based on simulations from the background state, reach +40 K to +50 K in the control run due to the use of a fixed sea ice surface emissivity of 0.8 for all channels and locations (Geer et al., 2022). Conversely, over the Antarctic continent, a fixed land surface emissivity of 0.95 used, which is far too high in many places, resulting in departures down to around -50 K. Panel b shows the observed brightness temperatures, with a strong contrast between ocean and sea ice surfaces, but also strong variability within these areas, coming from atmospheric effects (water vapour, cloud and precipitation) and surface effects (variable surface emissivity and skin temperature).

Figure 4c shows that after implementing the new sea ice emissivity model, the background departures from the sea ice regions are mostly within ±10K except in multi-year ice locations that will be discussed in the next section. The difference from the control departures is striking, and though it may seem that the control results could have been improved by using a more appropriate fixed channel-dependent surface emissivity in each channel, such a solution

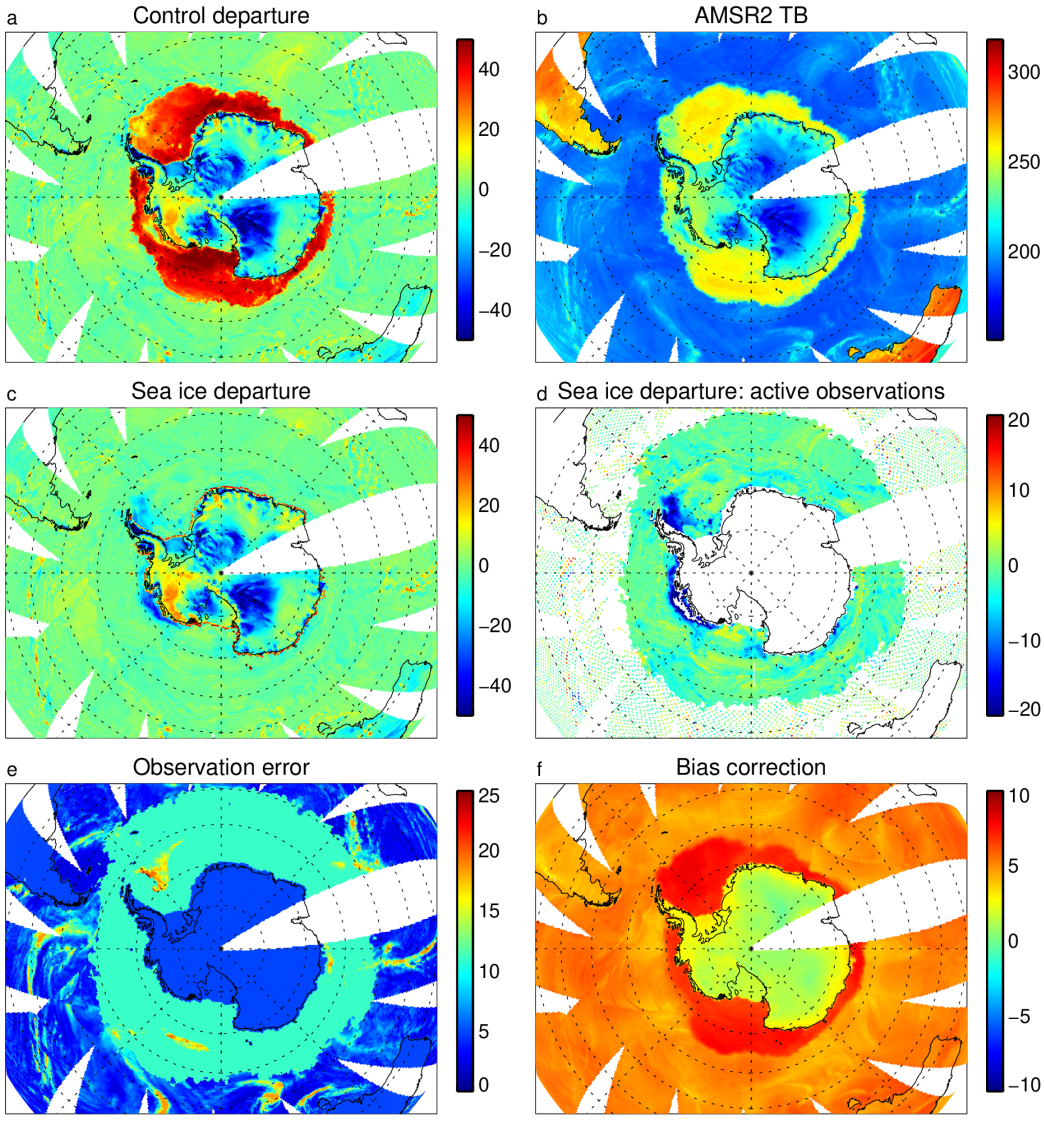

FIGURE 4 Utilisation of the 19v channel of AMSR2 in the 12 h assimilation window around 00 UTC 5th June 2022: a) background departure in the control experiment; b) Observed brightness temperature (TB); c) Background departure in the sea ice experiment; d) Background departure after thinning and screening; e) Observation error; f) Bias correction. All units are in Kelvin brightness temperature; multiple orbits run over each other in the polar regions, with the latest observation taking precedence in the plotting; all available superobs are shown (superpositions excepted) except in panel d.

did not exist in the IFS and would have been practically hard to achieve. As mentioned, there is strong dependence of sea ice emissivity on sea ice state, especially at higher frequencies and in horizontal polarisations, but even at 19v (e.g. Lee et al., 2017, their table 4). Therefore the difference between panels a and c is a reasonably fair illustration of the improvements available from the new model, compared to existing approaches in weather forecasting.

This work does not yet address snow and ice over land, so the departures over the Antarctic continent remain large. Figure 4d shows the observations selected for active use in data assimilation. Land areas are rejected completely in this channel. Over open ocean, only every 1 in 8 observations are used, leaving a rough diamond pattern of active data that is just visible at the resolution of the figure. In contrast, all observations are used in the sea ice pathway, at least for estimating surface properties, and this is indicated by the zone with denser observation coverage. The boundary of this zone follows the 277.0 K contour of SST. Some observations in the sea ice pathway have been lost to quality control in the region with background departures greater than around -20 K.

Figure 4e illustrates the observation error, which is variable dependent on the cloud amount in the open ocean areas. In the sea ice pathway the observation error is constant at 11 K in channel 19v (Table 2) except for a few areas where it reaches 15 - 25 K where relatively warm surface temperatures have led to 'summer scattering' observation error inflation (Eq. 3). It is also clear that the observation error in the sea ice pathway is almost always much larger than what is used over open ocean, which can be as low as 2.0 K in cloud-free areas. Note that the Antarctic land observation errors are not set to reasonable values as these areas are not used.

Figure 4f shows the bias correction, which is around +5 K over ocean areas and +8 K over sea ice, which follows the addition of the sea ice fraction as a bias predictor for AMSR2. This reflects known scene-dependent biases in the AMSR2 data (Geer et al., 2022; Berg et al., 2016). Bias variability over the ice is relatively small, but is larger over open ocean where it is mainly driven by variations in the skin temperature, wind speed and total column water vapour bias predictors. Note that the Antarctic land biases are not physically meaningful as the observations are not used there.

3.2 | Fitting the observations

For the active sea ice data from Fig. 4, Fig. 5 illustrates the ability of 4D-Var to fit the observations using the new sea ice approach. Bear in mind that the SIC has been retrieved prior to data assimilation using the 10v channel (Eq. 2), so any sea ice displacement errors have already been removed in the background departures. Had the OCEAN5 analysis been used as the background, there would have been errors as large as ±70K around the ice edge, reflecting the TB contrast between ocean and sea ice in this channel. As illustrated in a worst case scenario in Geer (2023) there can be errors of up to 1000 km in the position of the ice edge in OCEAN5. This is why the simple retrieval had to be used to provide a background SIC.

Since the SIC retrieval largely eliminates the ice edge displacement errors in the background departures, the remaining errors in Fig. 5 a and c largely come from an incorrect sea ice emissivity at background. The background values of the sea ice empirical state variables are all set to zero, so the sea ice surface emissivity starts out at the baseline value, which is roughly equivalent to an annual and global mean. Given these background departures, 4D-Var has the option of modifying the atmosphere, SIC or sea ice surface emissivity (through the empirical variables) in order to better fit the observations.

In the areas where 19v observations show background departures larger than -20 K (Fig. 5a), the analysis departures are typically within ±5 K (Fig. 5b). The improved fit to observations comes mainly by decreasing the sea ice surface emissivity (not shown). Figure 6 shows how the sea ice control variables at observation locations have adapted to help achieve this, by adjusting the empirical sea ice state variables 1 and 2 away from their initial values of zero and towards positive values (panels b and c). Following Geer (2023) these areas with strong negative departures are

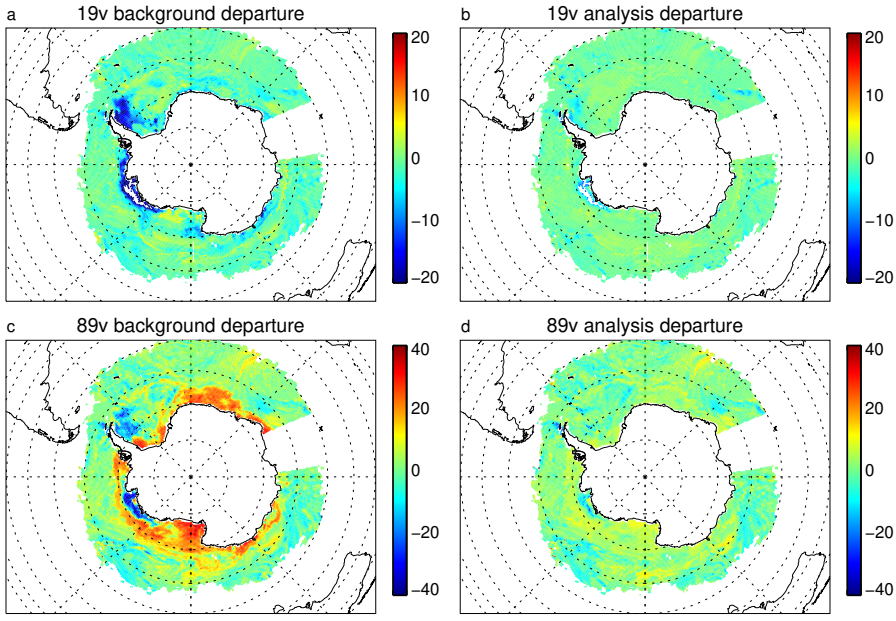

FIGURE 5 Background and analysis departure in Kelvin for AMSR2 channels 19v and 89v in the sea ice path in the 12 h assimilation window around 00 UTC 5th June 2022.

likely areas of longer-lived sea ice that will be described here as multi-year ice (MYI) though the exact age of the ice is unknown. In these areas, the sea ice generates strong scattering at microwave frequencies from air pockets within the ice (e.g. Warren, 2019). As further discussed in Geer (2023), the new sea ice emissivity model is not always fully able to fit the relatively low surface emissivity in MYI, meaning that sea ice concentrations can be pulled down incorrectly in order to fit the observations. As shown in panel a, there has also been a reduction in sea ice concentration by around 0.15. This is one of the main known problems of the new sea ice emissivity model and it means the SIC can be underestimated in winter MYI situations. Sec. 3.3 investigates further and proposes a correction strategy.

4D-Var is also able to fit the 89v observations in the Antarctic winter (Fig. 5c and d). While the 89v departures also show similar features in the MYI areas to the 19v observations, much of the sea ice area has positive background departures of up to around 30 K (panel c). These are likely areas of new ice where surface emissivities are relatively high at 89 GHz, due to the relative newness of the ice: for example it contains brine pockets rather than air bubbles, or it is physically smoother, and as well it is likely lacking any snow cover. In these areas, the empirical sea ice parameters are reduced to fit the observations, primarily the first parameter (Fig. 6b) as is expected in areas of new ice (Geer, 2023).

The summer months bring different challenges, as illustrated for the same day but in the Arctic in Fig. 7. Here, the background departures in the 19v channel are mostly well within ±10K, suggesting the 'baseline' surface emissivity values are reasonably good already, and the analysis departures reduce further, to within mostly around ±5K. However, at 89v, although some areas of positive background departures are better fit in the analysis, analysis departures remain larger than -20 K in many places. These are 'summer scattering' locations where the observation error has been boosted as high as 70 K to prevent these observations having much weight in the assimilation (not shown, see Eq. 3). These areas are down-weighted to prevent the quality of the atmospheric analysis being negatively affected, as was

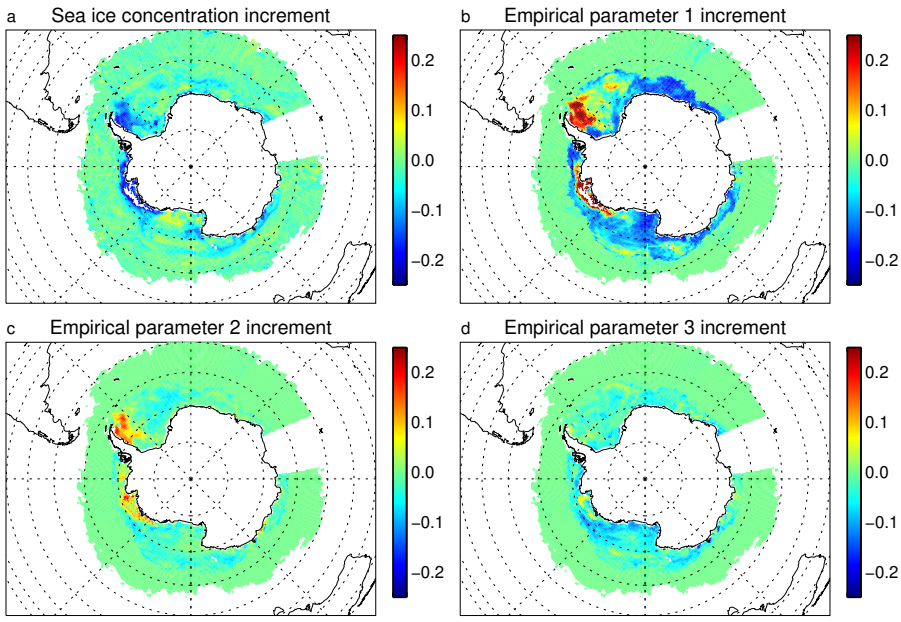

FIGURE 6 Increments in the observation-space control variables for AMSR2 observations in the sea ice path in the 12 h assimilation window around 00 UTC 5th June 2022.

seen in earlier trials. Additional investigations have shown that later in the Arctic summer, the problem is less well corrected due to relatively large observed brightness temperature depressions even at 19 GHz, which means the 19v-89v scattering index used to boost the observation error is less effective. This issue results in minor degradations in the Arctic late summer in the atmospheric forecast scores close to the north pole, but these degradations are localised in time and space, so that they do not show up in the annual statistics presented in Sec. 3.4.

3.3 | Sea ice quality

3.3.1 | Initial comparison to OCEAN5

Figure 8 concentrates on the SIC and its difference from the pre-existing OCEAN5 analysis (Zuo et al., 2019) interpolated to the observation locations. The differences between OCEAN5 and the AMSR2 background and analysis in 4D-Var are similar to what was already seen in the external machine learning study (Geer, 2023). The AMSR2 sea ice edge is much more sharply defined and shows smaller-scale features than OCEAN5 analysis. The precise location of the ice edge is also different by several hundred km, as illustrated in the difference plots (panels e and f). For example in the Bellingshausen and Amundsen seas (around 90°W) the AMSR2-based analysis shows more complete and extensive sea ice coverage, with the ice edge about 200 km further out than in OCEAN5. Around the Greenwich meridian, over a distance of about 500 km, OCEAN5 shows a much more gradual gradient in the SIC than in the AMSR2-based analysis. Around much of the rest of Antarctica, for example 90°E to 135°W, there are smaller disagreements in the location of the ice edge, with agreement within around 100 km.

Figure 8 also helps further illustrate some problems with the new SIC analysis, as was also found in the offline work

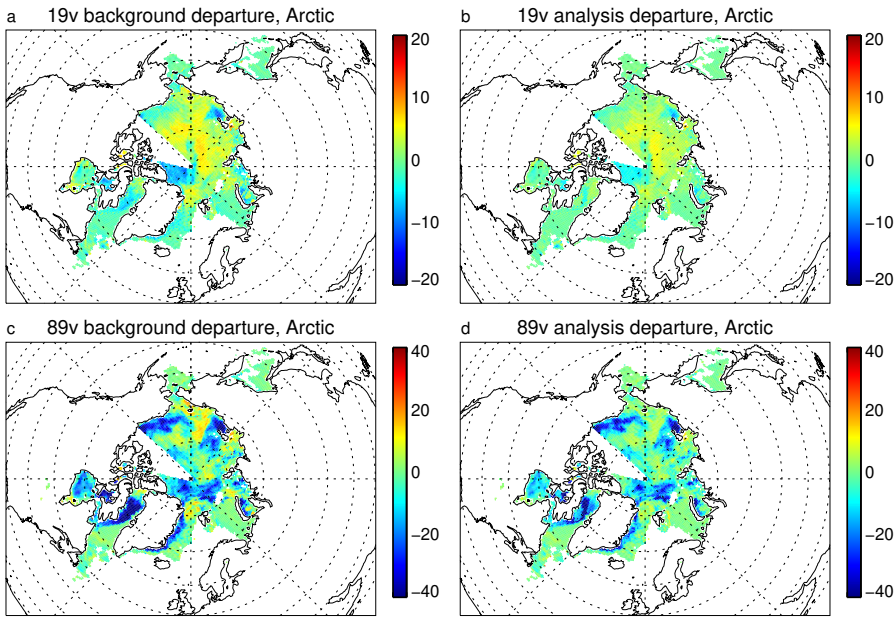

FIGURE 7 Background and analysis departure in Kelvin for AMSR2 channels 19v and 89v in the sea ice path in the 12 h assimilation window around 00 UTC 5th June 2022.

(Geer, 2023). The SIC in the AMSR2 analysis in the multi-year ice zones of the Bellingshausen sea and Weddel sea is around 0.1 to 0.2 lower than OCEAN5, due to the previously-mentioned problem with fitting the surface emissivity in these MYI regions. The background SIC is closer to OCEAN5 here, since the 10v channel is mostly unaffected by the issue. This fact is used as part of a correction strategy in the next section.

Another problem is the creation of areas of unphysical low SIC far beyond the main ice edge. These areas are obviously unphysical because sea ice, as opposed to icebergs, should quickly melt as it moves into warmer waters. The most extensive example is around 30°E, where a large area of the southern ocean is shown with SIC around 0.1 in both the background and the analysis. Similar features are seen at 100°W and 180°W. These areas are associated with the known problem of representing cold air outbreaks in the IFS (Lonitz and Geer, 2015; Forbes et al., 2016). These CAOs are airmasses moving equatorwards from the poles which typically combine strong winds, very low column water vapour, and boundary layer instability due to the relatively warm ocean surface. In reality this situation often generates supercooled liquid water cloud and rain but the IFS (in common with most models) is almost incapable of representing this. These areas are screened out in the usual ocean assimilation path but have been allowed in the sea ice path (Table 1). It is notable, however, that the spurious sea ice feature is similar in the background SIC and the analysis SIC. Since the background SIC is based only on the 10 GHz channel, which is thought to be mostly insensitive to atmospheric cloud and precipitation, this suggests that the problem is more than just the lack of supercooled liquid water in the forecast model, but also an issue of the ocean water surface emissivity modelling at low frequencies. This issue is under investigation and will be reported separately later.

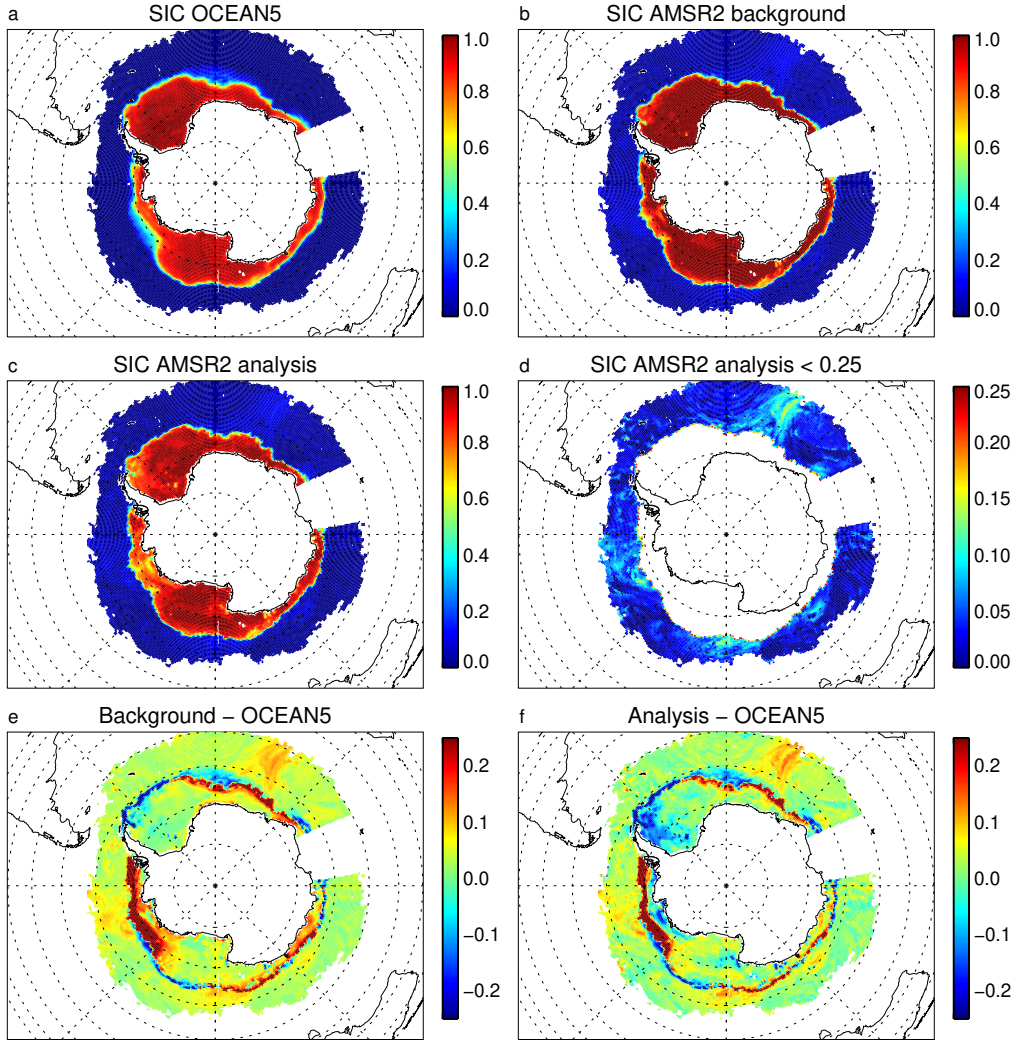

FIGURE 8 Sea ice concentration (SIC) at the AMSR2 observation locations in the sea ice path in the 12 h assimilation window around 00 UTC 5th June 2022: a) OCEAN5 analysis interpolated to AMSR2 locations; b) Background SIC in 4D-Var, retrieved from 10v channel; c) Analysis SIC in 4D-Var; d) As c but with zoomed-in scale for low SIC observations; e) Difference between background and OCEAN5; f) Difference between analysis and OCEAN5.

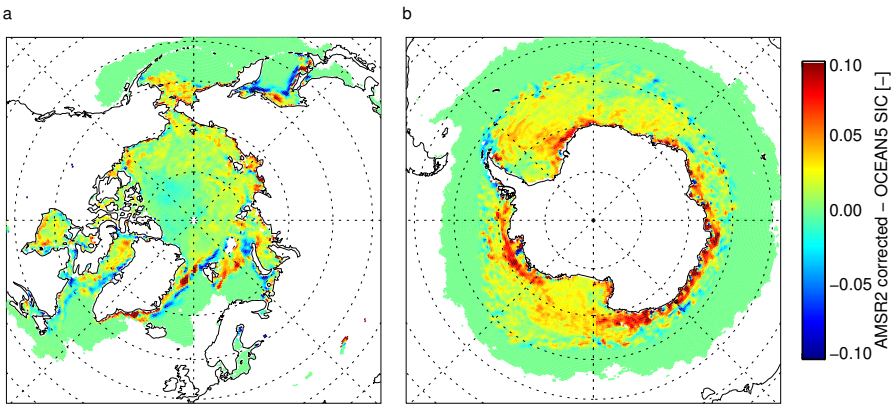

FIGURE 9 Mean difference in SIC between the corrected sea ice retrievals from AMSR2 and the OCEAN5 analysis at the same locations.

3.3.2 | Corrected sea ice concentration

Given the known issues with the new SIC retrievals produced by 4D-Var, some simple corrections are proposed to create an improved SIC product that would be suitable for assimilation into the ocean components at ECMWF (Zuo et al., 2019; Browne et al., 2019). The first issue to deal with is the underestimation of SIC in multi-year ice situations. As noted, in these locations the simple SIC retrieval which is used as the background, referred to here as $C_{ice,b}$ (Eq. 2), gives better results than the 4D-Var analysis, $C_{ice,a}$. Hence the following blending strategy is proposed, based on the value of the first empirical sea ice state variable, x_1, of which positive values typically indicate multi-year ice:

$$w = x_1/0.2; 0 \leq w \leq 1 \tag{5}$$

$$C_{ice,corrected} = (1 - w)C_{ice,a} + wC_{ice,b} \tag{6}$$

This ensures that zero or negative values of x_1 use the 4D-Var analysis $C_{ice,a}$ and values over 0.2 use entirely the background $C_{ice,b}$, with a smooth linear weighting in between. Following this blending, any SICs greater than 1 are reset to 1. Any SICs lower than 0.25 are reset to zero, since these are most likely spurious ice caused by unrepresented supercooled liquid cloud and rain in the model.

Using the corrected SIC, Fig. 9 shows the mean difference between the retrievals at AMSR2 locations and the OCEAN5 values interpolated to those locations, over the 2021 - 2022 testing period. Panel a shows that the MYI correction strategy has almost eliminated any mean discrepancies between the two SIC estimates in the Arctic, improving on the pure analysis product or the offline machine learning estimates (see Fig. 8 or Geer, 2023). The main discrepancies appear to be associated with the location of the ice edge, as would be expected. In the Antarctic, the new sea ice analysis shows slightly higher values than OCEAN5, but the main discrepancies are similar to those seen in the earlier work, with up to 0.1 higher SIC near the Antarctic continent. As examined in Geer (2023) this appears to be due to underestimation of the SIC in the OCEAN5 analysis in the Antarctic late summer.

As with the previous work Geer (2023) the primary advantage of the new sea ice analysis compared to OCEAN5

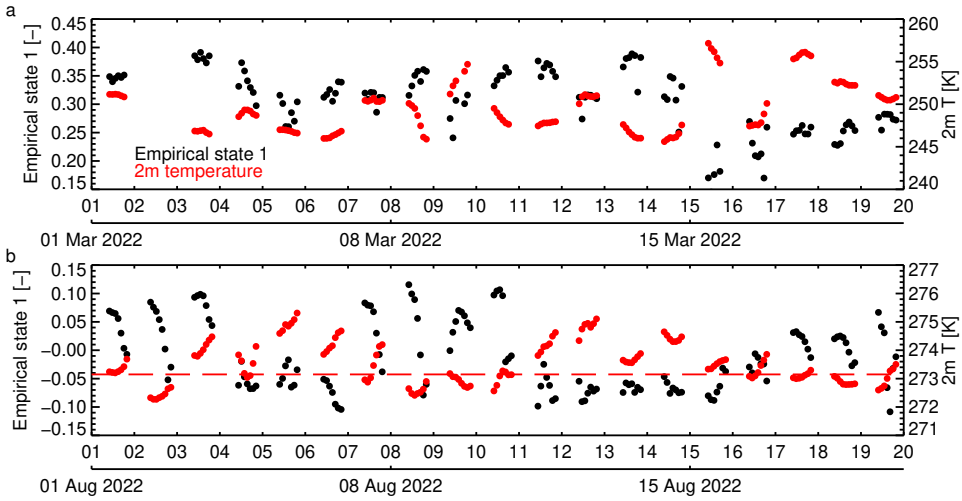

FIGURE 10 Extracts from the time series of AMSR2 superobs at 110°W, 80°N: a) late winter 2022; b) late summer 2022. All dates in UTC. Black dots show the 4D-Var analysis of empirical sea ice state variable 1 at the AMSR2 locations and red dots the 2m temperature at those locations estimated by the IFS model. The red dashed line indicates 273.15 K

is its timeliness, with OCEAN5 developing similar SIC patterns to the new analysis after a delay of approximately 48 h to 72 h. The drawbacks are the biases, mainly in MYI areas, and where cloud has been aliased as low concentration spurious sea ice, but these can be corrected as discussed here. Therefore the new sea ice analysis is expected to be overall substantially better than OCEAN5. However, it is not possible to find global high-quality validation data to assess that independently. Full validation of the new sea ice will come when it is used in cycling data assimilation experiments in place of the OSTIA sea ice analysis, where improved sea ice concentration should generate improved atmospheric and ocean forecasts.

3.3.3 | Sub-daily sea ice variability

The use of an observation space control variable in this work allows investigation of the sub-daily variability of the analysed SIC and the sea ice empirical properties. For a location in the Arctic multi-year ice at 110°W, 80°N, Fig. 10 shows time series of empirical variable 1 along with the 2m temperature, which seems to link with variations in the empirical sea ice properties (skin temperature, although it has a diurnal cycle, this is more static from day to day and does not seem to correlate as much). AMSR2's orbit means that latitudes polewards of around 75° degrees are observed up to around 7 times a day in a block of around 11 hours in duration, leading to a dense coverage of one part of the daily cycle followed by a large gap.

Fig. 10a shows a 20 day period at the end of winter, where air temperatures are around 245 - 255 K and the empirical state variable ranges from roughly 0.15 to 0.40. In this period, the empirical state is often quite stable within a day, and from day to day. The largest change is seen on 15th March, where the empirical variable was around 0.3 - 0.35 for many days and then suddenly dropped to around 0.2, followed by a gradual increase afterwards. The rise in temperature of 10 K between 14th and 15th March indicates a strong change in the weather and perhaps a wind event or a snow event that has changed the microstructural properties of the snow cover on top of the sea ice.

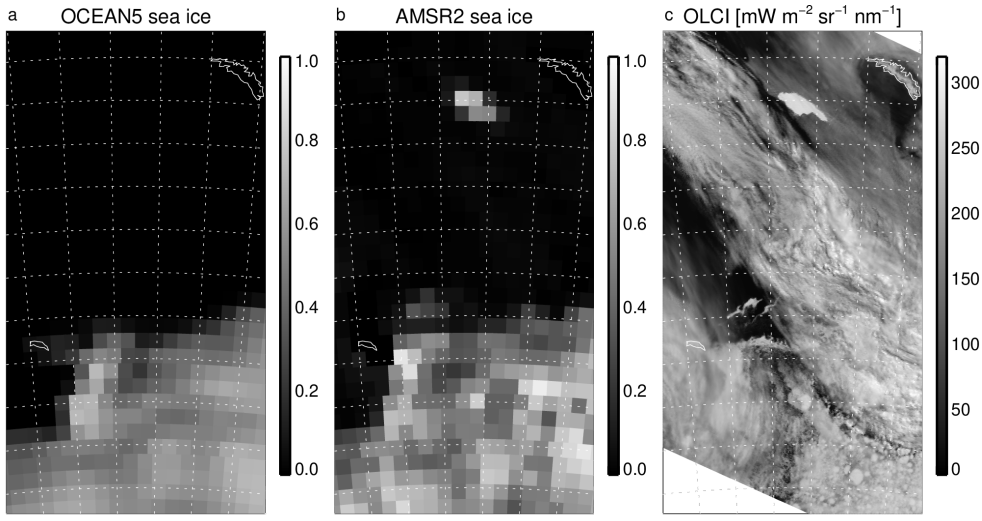

FIGURE 11 Sea ice in the Antarctic summer and the long-lived giant iceberg A68A at 12 UTC on 4th December 2020: (a): Current IFS sea ice fraction from the OCEAN5 analysis; (b) sea ice fraction at AMSR2 locations retrieved using the sea ice sink variable approach intended for 49R1; (c) OLCI visible radiances from channel 10 (681 nm) confirming the location of the giant iceberg. Grid lines are shown every 1° latitude and 2° longitude, along with the islands of South Georgia (top right) and one of the South Orkney group (centre left).

However, there is little apparent link betwee the empirical state variable and the atmospheric temperature otherwise.

Figure 10b shows a late summer example at the same location, where variations in the 2m atmospheric temperature are more closely linked to the state variable. The AMSR2 observations capture a period during the night and morning as air temperatures fall then rise. The value of the empirical state variable often reduces as the air temperature rises, particularly evident on 1 - 3 August and 17 - 19 August. There are also periods of air temperatures 1 to 2 K above freezing during 5 - 6 August and 12 - 14 August, and these seem to be associated with more stable values of the empirical state variable around -0.05, both within and between days. It could be speculated that this corresponds to wet snow on the sea ice, so that higher values of the empirical variable correspond to times when the snow re-freezes. The apparently strong within-day variability of the sea ice and snow microphysical properties, mainly in summer, shows that it is not sufficient to use daily average values. Hence this confirms the benefit of using the observation-space empirical control variables, until such time as models of the snow pack and sea ice can represent these changes in a physical way and with sufficient detail to be able to match the observations.

3.3.4 | Giant icebergs

To illustrate the quality of the sea ice concentration analysis on the 40 km (or 'pixel') scale of the AMSR2 superobs, Figure 11 focuses on December 2020, when the giant iceberg A68A[1] travelled from the Weddel Sea and past the island of South Georgia (Braakmann-Folgmann et al., 2022). This trajectory is well captured in the new sea ice concentration analyses for this period (not shown). The iceberg touched the sea bed close to South Georgia around December 17th

[1] Antarctic icebergs are numbered by the US National Ice Centre with the first letter indicating the region of origin and the any trailing letter used to identify fragments of an original iceberg.

and broke up completely over the following months (Huth et al., 2022). On December 5th it was described as oriented roughly NW-SE and was of order 100 km long and 60 km wide, parameters that fit closely with the analysed sea ice map (panel b) and visible imagery at the same time from Ocean and Land Colour Imager (OLCI, panel c). The OCEAN5 sea ice analysis (panel a) does not show any trace of A68A, though this is unsurprising given that long-lasting berg ice is not represented in the sea ice model in OCEAN5, let alone more generally in climate models, as discussed by Huth et al. (2022).

The representation of the main summer Antarctic ice pack is also captured in Fig. 11, towards the bottom of the domain. As seen also in Fig. 8, the new analysis appears sharper than OCEAN5, although many of the features are in common. Although the OLCI visible picture is heavily contaminated by cloud, it is possible to see some of the sea ice features below it, such as pancake-shaped bright spots on the scale of around 20 - 50 km (fractions of a grid box). The locations of these ice pancakes and also the dark areas without cloud or sea ice in the OCLI picture are, at least visually, often consistent with the AMSR2 sea ice analysis. There is also an an area of sea ice concentrations less than 0.5 that is seen in the AMSR2 analysis and not in OCEAN5, in the grid box NE of the one containing the South Orkney island. This appears to be colocated with a complex-shaped bright area in the OLCI data at the same location, which could be sea ice due to its distinctly different appearance compared to the cloud features elsewhere. It looks a lot like a streamer of high SIC less than around 10 km wide that has been separated from the main ice pack and has been deformed by ocean eddies on a similar scale. Similar qualitative agreement in the small-scale features of sea ice between OLCI and the AMSR2 analyses has been seen in other scenes with less cloud cover (not shown).

During the main test period in September and October 2022, another giant iceberg, A76A, was drifting clear of the sea ice in the Drake Passage. The US national ice centre (USNIC) estimated its size at 135 km by 26 km in May 2021 (`https://usicecenter.gov/PressRelease/IcebergA76A_B_C`) with a nearly rectangular shape giving approximately a 3510 km^2 surface area. The new AMSR2 analysis illustrates A76A being exposed by retreating sea ice around 10 September 2022 when it was on the edge of the Weddel Sea (no figure shown). Figure 12 shows the evolution of A76A over 24 days in October after it started to drift slowly northwards into the Drake Passage. The locations are consistent with those estimated by scatterometer and visible imagery recorded in the Antarctic iceberg tracking database (Budge and Long, 2018). The shape is long and narrow, occupying approximately 1 by 4 pixels or superobs, and is therefore consistent with the USNIC estimated dimensions. Between 11 and 30 October the AMSR2 analysis shows A76A rotating nearly 180 degrees clockwise, with a highly consistent shape throughout, accepting the pixellated nature of the analysis.

The area of iceberg A76A can be estimated roughly from the daily SIC figure by assuming each pixel or superob occupies 40 km by 40 km and then summing over a region of 90 pixels around the centre of the figure. The resulting estimate is shown as a timeseries at the bottom of Fig. 12 and is consistently close to 4000 km^2 except on 30 October, where an area of spurious sea ice appears, likely associated with a cold air outbreak. The slight overestimate compared to the USNIC measurements likely comes from contamination by low-concentration sea ice in areas of missing cloud, as discussed before. These calculations are based on the analysed SICs with values less than 0.1 treated as zero, slightly different to the usual recommendation of a 0.25 lower threshold, to preserve coverage of the iceberg, but at greater risk of being affect by spurious cloud. This aside, the day-to-day consistency of the shape and area of the iceberg should again give strong confidence in the pixel-level details shown in the new SIC analysis, as well as the ability of the all-sky radiance assimilation technique to provide continuous and reliable results despite frequent cloud cover.

The iceberg timeseries shown in Fig. 12 is highly novel, in that it is generated from passive microwave, rather than the visible imagery, scatterometer or SAR observations used more typically in this area (Budge and Long, 2018; Braakmann-Folgmann et al., 2022; Huth et al., 2022). The potential of the passive microwave for iceberg tracking

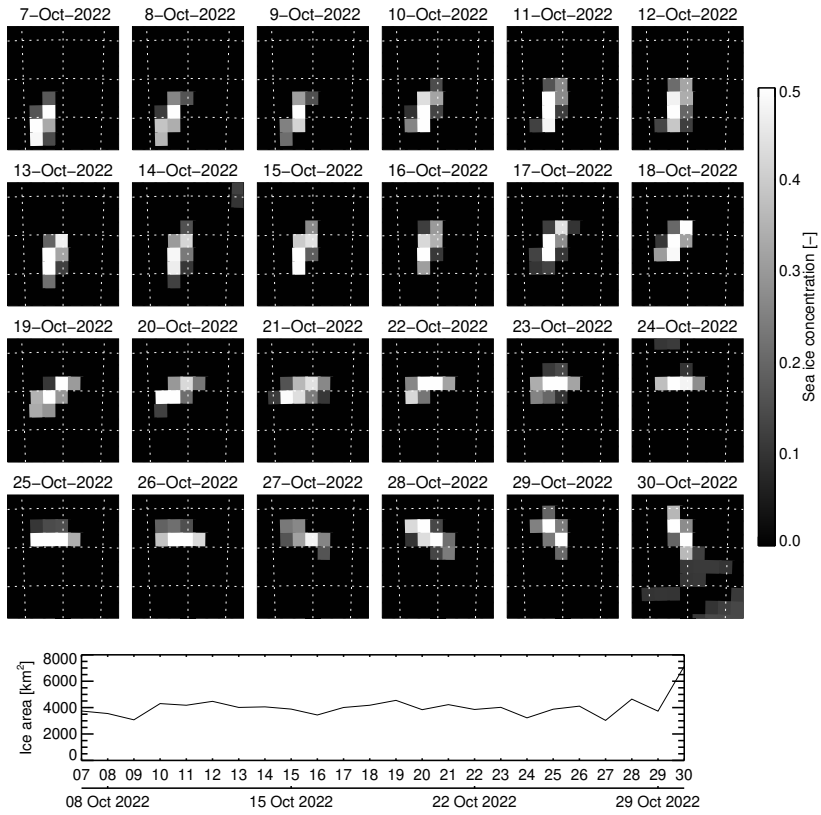

FIGURE 12 Daily maps of long-lived giant iceberg A76A during October 2022, based on the AMSR2 overpasses between 03 UTC and 05 UTC, and at the bottom, the estimated sea ice area for each overpass. Where multiple overpasses exist in the time window, the most recent measurement has been selected. Grid lines are shown every 1° latitude and 2° longitude and the projection is centred on 59.25°S 50°W. The analysed SIC is used in this plot with SIC values less than 0.1 reset to 0.0.

has long been clear, and there were early studies on the subject using hand analysis of the images (e.g. Phillips and Laxon, 1995) but it has not been developed further. The published A68A iceberg analyses (e.g Braakmann-Folgmann et al., 2022; Huth et al., 2022) mainly use visible imagery that nominally provides coverage every 1 – 2 days and sub-km resolution. However, high latitude locations are often cloudy, so visible imagery is not usable every day, and the reliance on daylight means that coverage may be entirely absent during the polar winter. Synthetic aperture radar (SAR) as used in e.g. Huth et al. (2022) is all-weather but is typically limited to a few overpasses per month. Scatterometers are sometimes used in order to provide more frequent coverage that is unaffected by cloud or sunlight conditions, and still with relatively good spatial resolution (e.g. around 5 km, Budge and Long, 2018). The new microwave-based analyses are available multiple times per day as illustrated in Figs. 2 and 3, with further advantages being their derivation through a quantitative and physical retrieval approach, as well as the relatively small effect of cloud. Although the current resolution is 40 km, which is worse than scatterometer analyses, the technique could be further developed to use the maximum resolution available in the AMSR2 data, also around 5 km in the 89 GHz channels (see

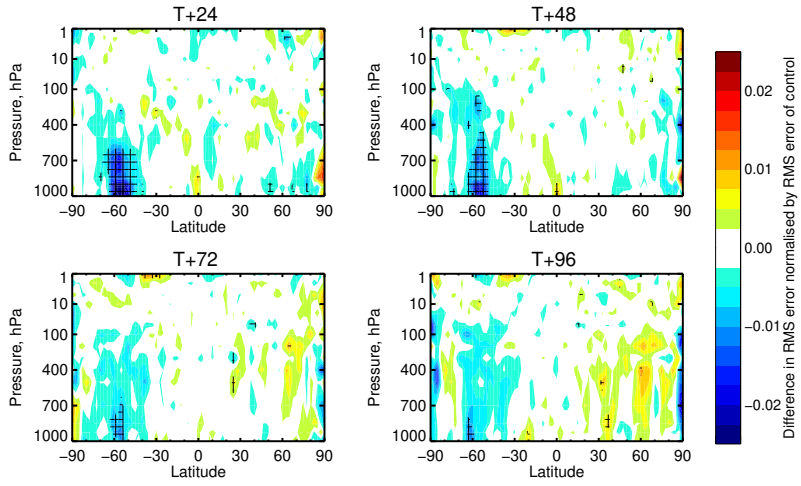

FIGURE 13 Change in RMS temperature forecast error between sea ice experiment and control, normalised by the RMS error of the control, over the 12 month testing period. Verification is against each experiment's own analysis. Cross hatching indicates statistical significance at the 95% confidence level, assuming each panel contains 20 independent tests. The notation "T+N" indicates the length of the forecast in hours, N.

e.g. Okuyama and Imaoka, 2015). Therefore the new sea ice technique for passive microwave could provide a useful new way of tracking giant icebergs. More generally, the focus on icebergs helps illustrate the high quality of the new analyses at the pixel level. This high quality likely carries over to all forms of sea ice.

3.4 | Forecast quality

Forecast quality is evaluated based on the year of experimentation between 1st November 2021 and 31st October 2022. Figure 13 shows the normalised change in RMS error in temperature when the sea ice assimilation is activated. The main beneficial impacts are at latitudes around 50 - 70°S and between the surface and around 500 hPa, lasting out to around day 4 of the forecast. Forecast quality is barely affected in the NH. The impact is clearest on the temperature field but other variables such as wind, humidity and geopotential height show similar impacts (not shown). The impact in the SH is strong enough to cause a statistically significant change in the southern hemisphere scores (20 to 90°S) of around 0.3% over the first 4 days of the forecast, strongest at 850 hPa (not shown).

The reduction in forecast errors is found mainly outside the areas directly affected by sea-ice, as indicated in Fig 14. Instead, the main reductions are centred around 55°S to 60°S, at the edge of the area where significant new data is being added from AMSR2 and GMI in areas that are mainly ice free (Figs. 2 and 3). Although the impact at 12 hours into the forecast could have propagated some distance from the original source in the analysis (by as much as hundreds of km) most likely the impact is coming from observations assimilated over ocean in the proximity of sea ice, rather than over the sea ice itself. This makes sense as the main storm tracks, which are typically the most sensitive locations for making forecast improvements (e.g. Rabier et al., 1996) tend to run over open ocean and not sea ice.

The impact on the background forecast fit to other observations could provide an alternative measure of the changes in forecast quality, but these are not investigated deelpy here. The changes are mostly non-significant, though with some rare statistically significant changes in quality within +0.2% and -0.2%, giving a broadly neutral effect on

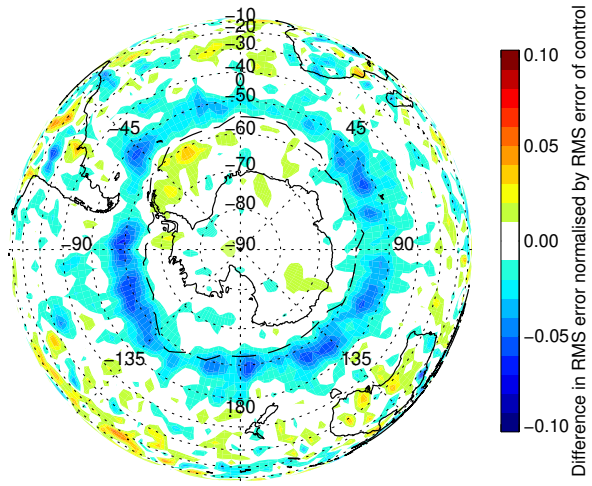

FIGURE 14 Normalised change in RMS temperature forecast error, as in Fig. 13, over the 12 months testing, but at 1000 hPa for the 12 h forecast (T+12). No statistical significance test is performed. The dashed line indicates the maximum sea ice extent based on a contour of SIC=0.5 in the September 2022 monthly mean.

these fits overall (not shown). This is probably to be expected, since the strongest impact on analysis-based forecast scores is in an area where there is little other coverage from satellite or ground-based observations.

4 | CONCLUSION

This study implements the empirical sea ice surface emissivity model from Geer (2023) within the atmospheric data assimilation system of ECMWF. The SIC and three empirical state variables are estimated at AMSR2 and GMI locations on a 40 km standardised (superobs) resolution. This allows the assimilation of microwave imager observations over sea ice areas for the first time, based on two principles:

- Accurate estimation of sea ice concentration in the footprint of the observation. This compares to the possible use of the SIC from the OCEAN5 analysis, which has errors in the location of the ice edge up to 200 km typically and in exceptional circumstances up to 1000 km, mainly due to being 48 h to 72 h behind reality (Geer, 2023).
- An ability to determine the sea ice emissivity across different frequencies and polarisations, despite the fact that the emissivity depends on poorly known surface properties such as the microphysical properties of the ice and overlying snow.

The ocean – sea ice contrast can lead to 150 K differences in brightness temperature in some channels, and the variation of surface emissivity can cause differences as large as 100 K. Hence the ability to simultaneously infer both the sea ice concentration and the surface emissivity is what makes the assimilation over sea ice possible. In the worst case with the new approach, in summertime freeze-thaw contexts at 89 GHz, the analysis departures can be as large as 20 K. But in most other contexts and channels, it is possible to fit the observations over sea ice within ±5 K at

analysis, which when compared to possible errors of ±150 K in the case of misplaced sea ice or natural variability in the sea ice emissivity, illustrates the power of the new technique.

The addition of new microwave imager observations at high latitudes improves the quality of atmospheric forecasts in the southern ocean, with statistical significance out to day 4. This comes in practice from filling observation gaps in areas of open ocean in the proximity of sea ice, rather than over the sea ice itself. The impact likely comes equally from AMSR2 and GMI, given the similar amount of new data being added at 55°S to 70°S, where the biggest forecast impacts are found.

The addition of observations at 55°S to 70°S is partly because the new sea ice framework allows microwave imager observations to be used in cold air outbreak (CAO) regions for the first time. In these regions, the forecast model struggles to represent supercooled liquid water clouds (Lonitz and Geer, 2015; Forbes et al., 2016), leading to the possibility of the assimilation not converging. By allowing the possibility of creating spurious low concentration sea ice (typically SICs around 0.1) the new approach acts as a pragmatic, if non-physical, safety valve in these areas. This highlights the importance of the CAO regions to forecast quality, which should justify the substantial future work required to improve the moist physics of the forecast model, along with improvements to the data assimilation system to create a more physically correct cloud and precipitation analysis in these areas. As well as adding CAO areas, the new framework more generally allows observations to be used confidently in places where sea ice might be found, where previously large numbers of observations would have been removed due to the risk of encountering sea ice.

The new sea ice assimilation will be used operationally in cycle 49r1 of the ECMWF weather forecasting system, which will go live in mid 2024. The SIC estimates from the atmospheric DA component will then be available for onward assimilation within the ocean component of the ECMWF system. This coupled data assimilation approach is already in testing and will be reported separately. When complete, we will be one step closer to eliminating the use of external sea ice retrieval products, with benefits to timeliness, robustness and quality of the sea ice analysis, as well as hopefully gaining further improvements in forecast quality through the coupling process (Browne et al., 2019; McNally et al., 2022).

The sea ice concentration analysis has some problems, including an underestimation of up to 0.15 in multi-year ice areas, as well as the aforementioned aliasing of missing supercooled liquid water cloud into the sea ice analysis. However, the first issue can be corrected by reverting to a simpler SIC retrieval based only on the 10v channel, and the latter issue can be corrected by treating all SICs less than 0.25 as open ocean. With these corrections applied, the mean SIC analysis agrees well with OCEAN5, except in the Antarctic summer where it appears the new analyses are better, and the OCEAN5 analysis has too little sea ice. The new analysis is valid at the observation time and location, and it shows much sharper features than OCEAN5. The sharpness differences are both on large scales (in one example OCEAN5 showed a shallow 500 km gradient in SIC where actually the sea ice edge was quite abrupt) and on the scales of the superobs used in the analysis, at 40 km.

In case studies of giant icebergs A68A and A76A, the new SIC analysis appears mostly correct at the pixel (40 km) resolution. The ability to track giant icebergs with passive microwave using a physically-based retrieval is novel. Although the spatial resolution is currently worse than existing techniques, this could be improved, and the ability to track icebergs automatically and reliably in all weather conditions, at daily or even more frequent time resolution, could provide genuinely new and useful information for maritime applications.

The analysed empirical sea ice state variables show the intended strong links with micro and macrostructural variability of sea ice and its snow cover. For example new ice and multi-year ice have distinct signatures (see also Geer, 2023). The sea ice state is strongly variable, particularly in the summer where variations often seem to follow the daily variations in near-surface air temperature, but also strongly variable from day to day with some apparent dependence on the weather. These changes likely drive (or are associated with) changes in snowpack moisture content

and crystalline structure. In order to move from an empirical to a physical description of the sea ice state when assimilating microwave radiance observations, a physical sea ice and snow model will need to be able to accurately simulate all of these characteristics, down to the microstructural details of the sea ice and its snow cover, as well as their temporal variability down to at least the hourly timescale.

The empirical sea ice surface emissivity model of Geer (2023) has been tested outside its training dataset for the first time in this work. The new testing uses a different time period, along with a different IFS model cycle from the one used in training, with one important difference being the use of a different ocean surface emissivity model. That the model worked without too many issues suggests that the empirical model is reasonably robust to interannual variability in sea ice conditions, as well as to changes in the surrounding model environment, and should not need retraining too often. However, the model does have problems, both in fitting multi-year ice conditions in winter, and in fitting strong scattering (or reflective) surfaces in summer, likely during daily freeze-thaw cycles. The model may be struggling to represent re-frozen snow situations. This latter issue may have arisen because the empirical model was trained on a daily average sea ice state, which could not represent the full sub-daily variability of summer sea ice surfaces.

Beyond the sea ice example, this work is the first demonstration of an approach that can be used to allow complete all-surface assimilation of satellite radiances. The new approach uses both empirical state variables and empirical model components, alongside physical models where they are accurate enough. This recognises that neither the surface state, nor the models that link that state to the observed radiances (observation operators), are yet represented well enough using purely physical approaches. The complex daily and sub-daily variability of the sea ice state suggests that it will be extremely challenging to do this with physical models. However, the semi-empirical approach can be easily and gradually adjusted to include more physical constraints as the relevant models get better.

The plan of future work extends in many of these directions:

- The representation of the surface radiative transfer as a skin temperature and surface emissivity is known to be problematic (e.g. Bormann et al., 2017), so the aim is to move away from this as soon as possible. The hope is to be able to represent the sub-surface radiative transfer more physically, following more advanced surface radiative transfer models (e.g. Picard et al., 2018; Sandells et al., 2023). However, it will likely be necessary to retain empirical modelling for the link between the state of the surface media and its optical properties.
- It is hoped to extend the empirical surface radiative transfer model to more surface types in its next retraining. The current approach should be relatively easy to extend over snow-covered land surfaces, given that the snow representation should be similar.
- The current validity range of the empirical model is frequencies between 10 and 89 GHz and zenith angles around 53°. To allow all microwave instruments to use empirical surface radiative transfer, this will need to be extended to higher frequencies (e.g. 183 GHz) and to allow a generalised angular dependence. This will be achieved by training against a wider range of microwave observations, but it likely also requires the more sophisticated radiative transfer physics to properly represent the angular (zenith angle) dependences.
- The current approach uses observation space augmented control variables, but it would be better to be able to directly share the high quality sea ice information obtained from microwave imagers with other sensors in the atmospheric analysis. This would be necessary so that, for example, microwave sounders can benefit from an improved surface description. This will likely require the use of model-space auxiliary control variable in the atmospheric 4D-Var following Massart et al. (2021) but it will be challenging to deal with the strong sub-daily variability of sea ice properties in that framework.
- The current framework does not retain sea ice state information from one analysis to the next, but it could be

beneficial to retain it. This again is more easily done with a model-space auxiliary control variable. Among many possible benefits, this could help extract more atmospheric information over sea ice. It could be done using a persistence model, by training an empirical prognostic model in the offline framework, or in the best case by using a physical sea ice model.

- Work is already in progress to assimilate the sea ice concentration in the ocean analysis by coupling the atmospheric data assimilation with the ocean (e.g. Browne et al., 2019) following existing work on assimilating skin temperature retrievals (McNally et al., 2022). This work aims to achieve the long term goal of replacing the use of externally-derived sea ice concentration products in the ocean analyses, hopefully improving the quality of the sea ice analysis and subsequently improving ocean and atmosphere forecast quality.

It is hoped that by rapidly improving the new all-sky all-surface assimilation framework following these principles, many of the existing problems can be addressed, and many new areas can be opened up, especially land surface applications.

acknowledgements

Niels Bormann, Tracy Scanlon, Stephen English, Phil Browne and Tony McNally are thanked for internal reviews of the manuscript.

references

Andersson, E. and Järvinen, H. (1998) Variational quality control. *Tech. Memo. 250*, ECMWF, Reading, UK.

Baordo, F. and Geer, A. (2015) Microwave surface emissivity over sea-ice. *EUMETSAT NWP-SAF visiting scientist report NWP-SAF_EC_VS_026*. URL: `https://nwpsaf.eu/publications/vs\_reports/nwpsaf-ec-vs-026.pdf`.

Baordo, F. and Geer, A. J. (2016) Assimilation of SSMIS humidity-sounding channels in all-sky conditions over land using a dynamic emissivity retrieval. *Quart. J. Roy. Meteorol. Soc.*, **142**, 2854–2866. URL: `https://doi.org/10.1002/qj.2873`.

Bauer, P., Thorpe, A. and Brunet, G. (2015) The quiet revolution of numerical weather prediction. *Nature*, **525**, 47–55.

Berg, W., Bilanow, S., Chen, R., Datta, S., Draper, D., Ebrahimi, H., Farrar, S., Jones, W. L., Kroodsma, R., McKague, D., Payne, V., Wang, J., Wilhiet, T. and Yang, J. X. (2016) Intercalibration of the GPM microwave radiometer constellation. *Journal of Atmospheric and Oceanic Technology*, **33**, 2639–2654. URL: `https://doi.org/10.1175/JTECH-D-16-0100.1`.

Bonavita, M., Isaksen, L., Hólm, E. and Fisher, M. (2016) The evolution of the ECMWF hybrid data assimilation system. *Quart. J. Roy. Meteorol. Soc.*, **142**, 287–303.

Bormann, N., Geer, A. and Bauer, P. (2011) Estimates of observation error characteristics in clear and cloudy regions for microwave imager radiances from NWP. *Quart. J. Roy. Meteorol. Soc.*, **137**, 2014–2023.

Bormann, N., Lupu, C., Geer, A., Lawrence, H., Weston, P. and English, S. (2017) Assessment of the forecast impact of surface-sensitive microwave radiances over land and sea-ice. *Tech. Memo. 804*, ECMWF, Reading, UK. URL: `https://doi.org/10.21957/qyh34roht`.

Braakmann-Folgmann, A., Shepherd, A., Gerrish, L., Izzard, J. and Ridout, A. (2022) Observing the disintegration of the a68a iceberg from space. *Rem. Sens. Env.*, **270**, 112855. URL: `https://doi.org/10.1016/j.rse.2021.112855`.

Browne, P. A., de Rosnay, P., Zuo, H., Bennett, A. and Dawson, A. (2019) Weakly coupled ocean–atmosphere data assimilation in the ECMWF NWP system. *Remote Sensing*, **11**, 234. URL: `https://doi.org/10.3390/rs11030234`.

Budge, J. S. and Long, D. G. (2018) A comprehensive database for Antarctic iceberg tracking using scatterometer data. *IEEE Journal of Selected Topics in Applied Earth Observations and Remote Sensing*, **11**, 434–442. URL: https://doi.org/10.1109/JSTARS.2017.2784186.

Buehner, M., Caya, A., Carrieres, T. and Pogson, L. (2016) Assimilation of ssmis and ascat data and the replacement of highly uncertain estimates in the environment canada regional ice prediction system. *Quarterly Journal of the Royal Meteorological Society*, **142**, 562–573. URL: https://doi.org/10.1002/qj.2408.

Chripko, S., Msadek, R., Sanchez-Gomez, E., Terray, L., Bessières, L. and Moine, M.-P. (2021) Impact of reduced arctic sea ice on northern hemisphere climate and weather in autumn and winter. *Journal of Climate*, **34**, 5847–5867. URL: https://doi.org/10.1175/JCLI-D-20-0515.1.

Dee, D. (2005) Bias and data assimilation. *Quart. J. Roy. Meteorol. Soc.*, **131**, 3323–3343.

Duncan, D., Bormann, N. and Geer, A. (2022) All-sky assimilation of AMSU-A window channels. *EUMETSAT/ECMWF Fellowship Programme Research Report 59*, ECMWF, Reading, UK. URL: https://doi.org/10.21957/daefm16p8.

Duncan, D., Bormann, N., Geer, A. and Weston, P. (2023) Superobbing and finer thinning for all-sky humidity sounder assimilation. *Tech. Memo. 905*, ECMWF, Reading, UK. URL: https://doi.org/10.21957/5c3b9c8d9f.

ECMWF (2023) IFS Documentation CY48R1. URL: https://www.ecmwf.int/en/forecasts/documentation-and-support/changes-ecmwf-model/ifs-documentation.

Eyre, J. R., English, S. J. and Forsythe, M. (2020) Assimilation of satellite data in numerical weather prediction. Part I: The early years. *Quart. J. Roy. Meteorol. Soc.*, **146**, 49–68. URL: https:/doi.org/10.1002/qj.3654.

Forbes, R., Geer, A., Lonitz, K. and Ahlgrimm, M. (2016) Reducing systematic errors in cold-air outbreaks. *ECMWF newsletter*, 17–22.

Geer, A. (2023) Simultaneous inference of sea ice state and surface emissivity model using machine learning and data assimilation. in preparation.

Geer, A. J., Baordo, F., Bormann, N. and English, S. (2014) All-sky assimilation of microwave humidity sounders. *Tech. Memo. 741*, ECMWF, Reading, UK. URL: https://doi.org/10.21957/obosmx154.

Geer, A. J., Baordo, F., Bormann, N., English, S., Kazumori, M., Lawrence, H., Lean, P., Lonitz, K. and Lupu, C. (2017) The growing impact of satellite observations sensitive to humidity, cloud and precipitation. *Quart. J. Roy. Meteorol. Soc.*, **143**, 3189–3206. URL: https:/doi.org/10.1002/qj.3172.

Geer, A. J., Lonitz, K., Duncan, D. and Bormann, N. (2022) Improved surface treatment for all-sky microwave observations. *Tech. Memo. 894*, ECMWF, Reading, UK. URL: https:/doi.org/10.21957/zi7q6hau.

Geer, A. J., Lonitz, K., Weston, P., Kazumori, M., Okamoto, K., Zhu, Y., Liu, E. H., Collard, A., Bell, W., Migliorini, S., Chambon, P., Fourrié, N., Kim, M.-J., Köpken-Watts, C. and Schraff, C. (2018) All-sky satellite data assimilation at operational weather forecasting centres. *Quart. J. Roy. Meteorol. Soc.*, **144**, 1191–1217.

Geer, A. J., Lupu, C. and co authors (2023) SURFEM-ocean microwave surface emissivity model evaluated in an opeational weather forecasting system. *Tech. Memo. in preparation*, ECMWF, Reading, UK.

Good, S., Fiedler, E., Mao, C., Martin, M. J., Maycock, A., Reid, R., Roberts-Jones, J., Searle, T., Waters, J., While, J. et al. (2020) The current configuration of the OSTIA system for operational production of foundation sea surface temperature and ice concentration analyses. *Remote Sensing*, **12**, 720. URL: https://doi.org/10.3390/rs12040720.

Hirahara, Y., Rosnay, P. d. and Arduini, G. (2020) Evaluation of a microwave emissivity module for snow covered area with CMEM in the ECMWF integrated forecasting system. *Remote Sensing*, **12**, 2946. URL: https://doi.org/10.3390/rs12182946.

Huth, A., Adcroft, A., Sergienko, O. and Khan, N. (2022) Ocean currents break up a tabular iceberg. *Science Advances*, **8**, eabq6974. URL: https://doi.org/10.1126/sciadv.abq6974.

Kazumori, M. (2016) Development of all-sky microwave radiance assimilation for JMA global NWP system. In *Proceedings for the 2016 EUMETSAT Meteorological Satellite Conference, 26–30 September 2016, Darmstadt, Germany*.

Kazumori, M. and English, S. J. (2015) Use of the ocean surface wind direction signal in microwave radiance assimilation. *Quarterly Journal of the Royal Meteorological Society*, **141**, 1354–1375. URL: https://doi.org/10.1002/qj.2445.

Kilic, L., Prigent, C., Jimenez, C., Turner, E., Hocking, J., English, S., Meissner, T. and Dinnat, E. (2023) Development of the SURface Fast Emissivity Model for Ocean (SURFEM-Ocean) based on the PARMIO radiative transfer model. *Earth and Space Science*, **10**, e2022EA002785. URL: https://doi.org/10.1029/2022EA002785.

Kunkee, D., Poe, G., Boucher, D., Swadley, S., Hong, Y., Wessel, J. and Uliana, E. (2008) Design and evaluation of the first Special Sensor Microwave Imager/Sounder. *IEEE Trans. Geosci. Remote Sensing*, **46**, 863–883. URL: https://doi.org/10.1109/TGRS.2008.917980.

Lawrence, H., Bormann, N., Sandu, I., Day, J., Farnan, J. and Bauer, P. (2019) Use and impact of Arctic observations in the ECMWF numerical weather prediction system. *Quart. J. Roy. Meteorol. Soc.*, **145**, 3432–3454. URL: https://doi.org/10.1002/qj.3628.

Lean, P., Geer, A. and Lonitz, K. (2017) Assimilation of Global Precipitation Mission (GPM) Microwave Imager (GMI) in all-sky conditions. *Tech. Memo. 799*, ECMWF, Reading, UK. URL: https://doi.org/10.21957/8orc7sn33.

Lean, P., Hólm, E., Bonavita, M., Bormann, N., McNally, A. and Järvinen, H. (2021) Continuous data assimilation for global numerical weather prediction. *Quarterly Journal of the Royal Meteorological Society*, **147**, 273–288.

Lee, S.-M., Sohn, B.-J. and Kim, S.-J. (2017) Differentiating between first-year and multiyear sea ice in the arctic using microwave-retrieved ice emissivities. *J. Geophys. Res.: Atmos.*, **122**, 5097–5112. URL: https://doi.org/10.1002/2016JD026275.

Lonitz, K. and Geer, A. (2015) New screening of cold-air outbreak regions used in 4D-Var all-sky assimilation. *EUMETSAT/ECMWF Fellowship Programme Research Report 35*, ECMWF, Reading, UK.

Lonitz, K., Geer, A. J. and Bormann, N. (2022) Towards assimilating microwave imager channels over land. *EUMETSAT/ECMWF Fellowship Programme Research Report 58*, ECMWF, Reading, UK. URL: https://doi.org/10.21957/gdwqzfns.

Massart, S., Bormann, N., Bonavita, M. and Lupu, C. (2021) Multi-sensor analyses of the skin temperature for the assimilation of satellite radiances in the European Centre for Medium-range Weather Forecasts (ECMWF) Integrated Forecasting System (IFS, cycle 47R1). *Geoscientific Model Development*, **14**, 5467–5485. URL: https://doi.org/10.5194/gmd-14-5467-2021.

McNally, A. (2009) The direct assimilation of cloud-affected satellite infrared radiances in the ECMWF 4D-Var. *Quart. J. Roy. Meteorol. Soc.*, **135**, 1214–1229.

McNally, T., Browne, P., Chrust, M., Fairbairn, D., Massart, S., Mogensen, K. and Zuo, H. (2022) Progress on developing a new coupled sea-surface temperature analysis. *ECMWF Newsletter*, 17–22. URL: https://doi.org/10.21957/tm4913hs8d.

Meissner, T., Wentz, F., Lindsley, R., Wentz, K. and Mears, C. (2023) Overview of the WSF-M ocean surface vector winds and sea ice algorithms. In *IGARSS 2023 - 2023 IEEE International Geoscience and Remote Sensing Symposium*. URL: https://doi.org/10.1109/IGARSS52108.2023.10281455.

Migliorini, S., Piccolo, C. and Rodgers, C. D. (2008) Use of the information content in satellite measurements for an efficient interface to data assimilation. *Mon. Weath. Rev.*, **136**, 2633–2650.

Mu, L., Nerger, L., Tang, Q., Loza, S. N., Sidorenko, D., Wang, Q., Semmler, T., Zampieri, L., Losch, M. and Goessling, H. F. (2020) Toward a data assimilation system for seamless sea ice prediction based on the AWI climate model. *Journal of Advances in Modeling Earth Systems*, **12**, e2019MS001937. URL: https://doi.org/10.1029/2019MS001937.

Okuyama, A. and Imaoka, K. (2015) Intercalibration of advanced microwave scanning radiometer-2 (AMSR2) brightness temperature. *IEEE Transactions on Geoscience and Remote Sensing*, **53**, 4568–4577. URL: https://doi.org/10.1109/TGRS.2015.2402204.

Phillips, H. and Laxon, S. (1995) Tracking of antarctic tabular icebergs using passive microwave radiometry. *Remote Sensing*, **16**, 399–405. URL: https://doi.org/10.1080/01431169508954407.

Picard, G., Sandells, M. and Löwe, H. (2018) SMRT: An active–passive microwave radiative transfer model for snow with multiple microstructure and scattering formulations (v1. 0). *Geoscientific Model Development*, **11**, 2763–2788.

Rabier, F., Klinker, E., Courtier, P. and Hollingsworth, A. (1996) Sensitivity of forecast errors to initial conditions. *Quart. J. Roy. Meteorol. Soc.*, **122**, 121–150.

de Rosnay, P., Browne, P., de Boisséson, E., Fairbairn, D., Hirahara, Y., Ochi, K., Schepers, D., Weston, P., Zuo, H., Alonso-Balmaseda, M., Balsamo, G., Bonavita, M., Bormann, N., Brown, A., Chrust, M., Dahoui, M., Chiara, G. D., English, S., Geer, A., Healy, S., Hersbach, H., Laloyaux, P., Magnusson, L., Massart, S., McNally, T., Pappenberger, F. and Rabier, F. (2022) Coupled assimilation at ECMWF: current status, challenges and future developments. *Quart. J. Roy. Meteorol. Soc.*, **148**, 2672—-2702. URL: https://doi.org/10.1002/qj.4330.

Sandells, M., Rutter, N., Wivell, K., Essery, R., Fox, S., Harlow, C., Picard, G., Roy, A., Royer, A. and Toose, P. (2023) Simulation of arctic snow microwave emission in surface-sensitive atmosphere channels. *EGUsphere*, **2023**, 1–28. URL: https://egusphere.copernicus.org/preprints/2023/egusphere-2023-696/.

Saunders, R., Hocking, J., Turner, E., Rayer, P., Rundle, D., Brunel, P., Vidot, J., Roquet, P., Matricardi, M., Geer, A., Bormann, N. and Lupu, C. (2018) An update on the RTTOV fast radiative transfer model (currently at version 12). *Geosci. Model Dev.*, **11**, 2717–2737.

Scanlon, T., Geer, A. and Bormann, N. (2023) Microwave imagers in the ECMWF-IFS: Adding further observations and improving convective anvils in the observation operator. *EUMETSAT/ECMWF Fellowship Programme Research Report 61*, ECMWF, Reading, UK. URL: https://doi.org/10.21957/8542a37c46.

Timmermann, R., Goosse, H., Madec, G., Fichefet, T., Ethe, C. and Duliere, V. (2005) On the representation of high latitude processes in the ORCA-LIM global coupled sea ice–ocean model. *Ocean Modelling*, **8**, 175–201. URL: https://doi.org/10.1016/j.ocemod.2003.12.009.

Warren, S. G. (2019) Optical properties of ice and snow. *Philosophical Transactions of the Royal Society A*, **377**, 20180161. URL: https://doi.org/10.1098/rsta.2018.0161.

Zampieri, L., Arduini, G., Holland, M., Keeley, S. P., Mogensen, K., Shupe, M. D. and Tietsche, S. (2023) A machine learning correction model of the winter clear-sky temperature bias over the Arctic sea ice in atmospheric reanalyses. *Monthly Weather Review*, **151**, 1443–1458. URL: https://doi.org/10.1175/MWR-D-22-0130.1.

Zuo, H., Balmaseda, M. A., Tietsche, S., Mogensen, K. and Mayer, M. (2019) The ECMWF operational ensemble reanalysis–analysis system for ocean and sea ice: a description of the system and assessment. *Ocean science*, **15**, 779–808. URL: https://doi.org/10.5194/os-15-779-2019.